Lab on a Chip

CRITICAL REVIEW

View Article Online
View Journal

Cite this: DOI: 10.1039/c9lc00785g

Focusing of sub-micrometer particles in microfluidic devices

Tianlong Zhang,[ab] Zhen-Yi Hong,[a] Shi-Yang Tang,[c] Weihua Li,[c] David W. Inglis,[b] Yoichiroh Hosokawa,[a] Yaxiaer Yalikun*[a] and Ming Li*[b]

Sub-micrometer particles (0.10–1.0 μm) are of great significance to study, *e.g.*, microvesicles and protein aggregates are targets for therapeutic intervention, and sub-micrometer fluorescent polystyrene (PS) particles are used as probes for diagnostic imaging. Focusing of sub-micrometer particles – precisely control over the position of sub-micrometer particles in a tightly focused stream – has a wide range of applications in the field of biology, chemistry and environment, by acting as a prerequisite step for downstream detection, manipulation and quantification. Microfluidic devices have been attracting great attention as desirable tools for sub-micrometer particle focusing, due to their small size, low reagent consumption, fast analysis and low cost. Recent advancements in fundamental knowledge and fabrication technologies have enabled microfluidic focusing of particles at sub-micrometer scale in a continuous, label-free and high-throughput manner. Microfluidic methods for the focusing of sub-micrometer particles can be classified into two main groups depending on whether an external field is applied: 1) passive methods, which utilize intrinsic fluidic properties without the need of external actuation, such as inertial, deterministic lateral displacement (DLD), viscoelastic and hydrophoretic focusing; and 2) active methods, where external fields are used, such as dielectrophoretic, thermophoretic, acoustophoretic and optical focusing. This article mainly reviews the studies on the focusing of sub-micrometer particles in microfluidic devices over the past 10 years. It aims to bridge the gap between the focusing of micrometer and nanometer scale (1.0–100 nm) particles and to improve the understanding of development progress, current advances and future prospects in microfluidic focusing techniques.

Received 9th August 2019,
Accepted 6th November 2019

DOI: 10.1039/c9lc00785g

rsc.li/loc

1. Introduction

Particle focusing, conventionally defined as either two-dimensional (2D) focusing, where particles are horizontally focused at the center-plane of a microchannel, or three-dimensional (3D) focusing, in which particles are focused not only horizontally but also vertically, always serves as a prerequisite step for downstream processing, such as detection, separation and manipulation of target particles.[1,2] Moreover, the ability to position particles (both biological and synthetic) in a tightly focused stream is important for flow cytometry, imaging flow cytometry[3–5] and deformability cytometry.[6,7] The position of focused particles is not necessarily limited to a single position in the channel center, and multiple focal positions may also exist. For example, multiple streamline particle focusing occurs when using inertial forces to direct particles towards sidewalls of a square microchannel.[8] Microfluidic devices feature low reagent consumption, small size, fast analysis and low cost,[9,10] allowing them to act as ideal platforms for particle focusing, concentration and separation in a wide range of fields, such as biology, chemistry and medical science.[11–15]

Sub-micrometer particles with specific physical and biochemical properties, such as superconducting particles, normal mitochondria, infectious airborne viruses, *etc.*, are of great significance to study.[16–21] In this review, sub-micrometer and nanometer particles are defined as the particles with size ranging from 0.10 to 1.0 μm and 1.0 to 100 nm, respectively, to avoid confusion.[22–25] Due to the biomedical, environmental and industrial significance of sub-micrometer particles, precisely control over their positions in one or multiple focal streams has diverse applications, *e.g.*, clinical diagnosis, environmental monitoring, food analysis and drug delivery.[26–28]

Microvesicles (0.10–1.0 μm), a type of extracellular vesicles generated by budding or blebbing of the plasma membrane, have essential regulatory roles in the progress of rheumatoid arthritis and oncogenic processes, such as tumor proliferation

[a] *Division of Materials Science, Nara Institute of Science and Technology, Nara 630-0192, Japan. E-mail: yaxiaer@ms.naist.jp*
[b] *School of Engineering, Macquarie University, Sydney 2122, Australia. E-mail: ming.li@mq.edu.au*
[c] *School of Mechanical, Materials, Mechatronic and Biomedical Engineering, University of Wollongong, Wollongong 2522, Australia*

and invasion.[29–32] Moreover, microvesicles can be used for macromolecular drug delivery.[29] Protein aggregates (*e.g.*, immune complexes) with a similar size to microvesicles[30,33] play a vital role in neurodegenerative disease progressions, such as Alzheimer's disease and prion diseases, making them as targets for therapeutic treatment.[34,35] Geometrically encoded fluorescent barcodes self-assembled from DNA (0.40–0.80 μm) are used as *in situ* single-molecule probes, *e.g.*, the tags for labeling proteins on yeast cell surface.[36] Some bacteria in sub-micrometer range can be either harmful or beneficial to humans and the environment. For example, *Staphylococcus aureus* (*S. aureus*) is one of the major causes of skin, soft-tissue, bone, joint and endovascular disorders, while *Staphylococcus epidermidis* (*S. epidermidis*) is beneficial by balancing epithelial microflora with immune tolerance.[37,38] *Prochlorococcus* (0.50–0.70 μm), the most abundant photosynthetic organism on the planet, is of global significance due to its crucial role in the marine carbon cycle.[39–44] Sub-micrometer fluorescent polystyrene (PS) particles are used as fluorescent probes for diagnosis, imaging and optical tracking,[45] as PS is hardly biodegradable and does not show any short-term cytotoxicity in cellular environment.[46] A study by Rogach *et al.* showed that sub-micrometer PS particles can be coated with luminescent crystals, indicating their potentials for telecommunication applications.[47]

A variety of techniques for the focusing of sub-micrometer particles in microfluidic devices have been developed. These techniques were previously classified as either 1) sheath flow focusing which employs sheath fluids to pinch suspending particles to the center of the channel or 2) sheathless focusing, where a force driving particles laterally to their equilibrium positions is applied.[2,48] To elucidate the various focusing approaches and their mechanisms, in this review,

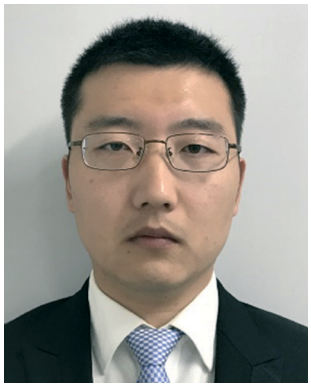

Tianlong Zhang

Tianlong Zhang received a bachelor's degree in engineering and master's degree in engineering from Jilin University, China in 2014 and 2017, respectively. He is currently a cotutelle PhD candidate in Division of Materials Science at Nara Institute of Science and Technology (NAIST), Japan and School of Engineering at Macquarie University, Australia. His research interests include microfluidics, cell mechanics, cancer metastasis and laser processing.

Weihua Li

Weihua Li, PhD, is a Senior Professor and Director of the Advanced Manufacturing Research Strength at the University of Wollongong, Australia. His research focuses on smart materials and their applications, microfluidics, lab on a chip, rheology, and intelligent mechatronics. He serves as editor or editorial board member for more than 11 international journals. He has published more than 280 journal papers. He is a recipient of Fellow of the Engineers Australia, the Fellow of Institute of Physics (UK), Australian Endeavour Research Fellowship, JSPS Invitation Fellowship, Vice-Chancellor's Award for Interdisciplinary Research Excellence, and Vice-Chancellor's Award for Excellence in Research Supervision.

David W. Inglis

Dr David W. Inglis received a BSc in Engineering Physics from The University of Alberta in 2001 and a PhD in Electrical Engineering from Princeton University in 2007. He is now a Senior Lecturer in the School of Engineering at Macquarie University in Sydney Australia. His research interests lie in microfabrication for medicine and biology and is known for work on deterministic lateral displacement.

Yoichiroh Hosokawa

Yoichiroh Hosokawa is a Professor in the Division of Materials Science, Nara Institute of Science and Technology, Japan. He is also a Joint Associate Professor in the Institute of BioPhotonics, National Yang Ming University, Taiwan. He received a Ph.D. in Applied Physics from Osaka University, Japan. His interest is in investigation of strong photo-excitation phenomena induced by intense ultra-short pulse lasers and their applications to manipulation and analysis of biological cells in microfluidic chips.

we categorize microfluidic techniques for sub-micrometer particle focusing into two main groups: active and passive focusing. The active techniques require an external field such as electric, acoustic and thermal field to provide a driving force to focus particles, in contrast, the passive techniques only rely on the intrinsic properties of fluids within channels.

With a focus on the studies over the past 10 years, this review mainly summarizes two main groups of microfluidic techniques for the focusing of sub-micrometer particles: 1) passive focusing (*e.g.*, inertial, DLD, viscoelastic and hydrophoretic focusing) and 2) active focusing techniques (*e.g.*, dielectrophoresis, DEP, acoustophoresis, thermophoresis and optical tweezers). Fig. 1 schematically illustrates these techniques and their focusing performance. For each technique, we provide a definition and briefly introduce its theoretical fundamentals. Representative studies on sub-micrometer particle focusing in microfluidic devices using this technique are described and typical figures are presented to facilitate the understanding of focusing mechanisms, dynamic processes and applications. The advantages and disadvantages of each focusing technique are discussed. We also talk about main challenges in sub-micrometer particle focusing and provide design guidelines of each technique for researchers in both academia and industry. A table summarizing key characteristics of each technique, *e.g.*, focusing criteria, methods, typical samples, merits and demerits, is presented at the end. Given the importance of sub-micrometer particles for various biological, biomedical and environmental applications, we aim to promote the understanding of the development process, current advances and future prospects of microfluidic techniques for the focusing of particles at sub-micrometer scale.

2. Passive methods

Passive microfluidic techniques depend on the intrinsic properties of fluids to achieve particle focusing, and they do not rely on external fields to provide driving forces. In this section, three types of passive microfluidic techniques for the focusing of sub-micrometer particles are discussed, namely inertial microfluidics, viscoelastic microfluidics and DLD, which mainly rely on inertial lift forces, viscoelastic forces and pillar-induced hydrodynamic forces to achieve the focusing.

2.1 Inertial microfluidics

Inertial focusing uses the inertial lift forces (*e.g.*, wall lift force and shear lift force) to drive particles to one or multiple equilibrium positions in a microchannel (Fig. 1a). In general, the wall lift force directs the particle away from the wall and decays with the distance from the wall, while the shear lift force drives the particle towards the wall and is zero at the channel centerline.[49] In a straight microchannel, the net lift force (F_L) on a particle can be expressed as below,[50]

$$F_L = \frac{\rho v m^2 d^4}{{D_h}^2} f_c \quad (1)$$

where ρ, v_m, d, D_h, and f_c indicate fluid density, maximum channel velocity, particle diameter, channel hydraulic diameter and lift coefficient. As shown in eqn (1), the net lift force will decrease significantly with small decrease in particle size due to the fourth-order dependence. To overcome this effect and achieve focused particle stream, relatively small cross sections and large velocities are always required.

Inertial focusing has been widely used for the manipulation of micrometer particles (*e.g.*, mammalian cells and microalgae cells),[51,52] but the focusing of particles at sub-micrometer scale encounters challenges as the required minimum length of the microchannel for effective focusing increases dramatically with the decrease of the particle size.[49,53] Only in recent years, inertial focusing devices see

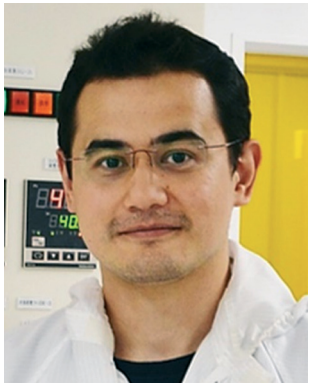

Yaxiaer Yalikun

Dr Yaxiaer Yalikun received his Ph.D. degree from Osaka University, Japan, in 2014. He worked as a specially appointed assistant professor in the Department of Mechanical Engineering, Graduate School of Engineering, Osaka University, from 2014 to 2015. He held the position of Postdoctoral Researcher in the Quantitative Biology Center, RIKEN, Japan, from 2015 to 2018. He is an Associate Professor at the Nara Institute of Science and Technology since 2018, where he specialized in fabrication of micro/nano devices and femtosecond laser manipulation.

Ming Li

Dr Ming Li is currently a Lecturer in the School of Engineering at Macquarie University in Sydney, Australia. She competed her PhD in Mechanical Engineering at the University of Wollongong, Australia in 2013. She was a postdoctoral research fellow in the Department of Bioengineering and Department of Electrical Engineering at the University of California, Los Angeles, USA from 2014 to 2017, and Department of Electrical and Computer Engineering at the University of Houston, USA from 2013 to 2014. Her research interests include microfluidics, plasmonic biosensors, lab-on-a-chip devices and cytometry.

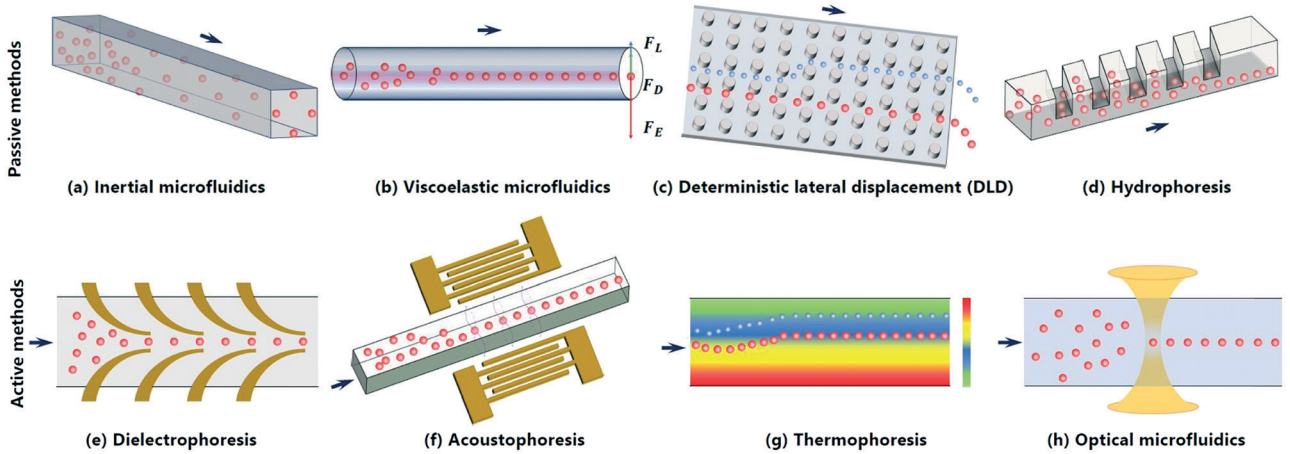

Fig. 1 Schematic illustration of passive and active microfluidic techniques for the focusing of sub-micrometer particles. Passive methods utilize intrinsic fluidic properties without the need for external actuation, such as (a) inertial, (b) viscoelastic, (c) deterministic lateral displacement (DLD) and (d) hydrophoretic focusing; while active methods such as (e) dielectrophoretic, (f) acoustophoretic, (g) thermophoretic and (h) optical focusing, require external fields.

the advances of focusing resolution from micrometer to sub-micrometer scale. After providing a theoretical approach for the design of a curved microchannel, Cruz *et al.* experimentally demonstrated label-free, continuous and high-throughput inertial focusing of 1.0 μm PS particles and sub-micrometer *Escherichia coli* (*E. coli*) at a flow rate of 50 μL min^{-1}.[54] In this work, the authors firstly analyzed the correlations between scale factors, such as particle size, hydraulic diameter, fluid speed and focus length, secondly scaled down the size of the particles by adjusting these scale factors, and lastly provided experimental validations. Further optimization of channel geometry for focusing is important in inertial microfluidics due to its features such as simplicity of use and high-throughput performance.

In 2017, Wang *et al.* demonstrated that 0.92 μm PS particles can be focused to equilibrium positions at a flow rate of 500 μL min^{-1} in a serpentine microchannel.[50] This channel consists of five functional components (Fig. 2a), namely 1) an inlet to introduce homogeneous suspensions, 2) a filter region to prevent channel clogging by trapping larger particles, 3) an asymmetric serpentine channel to focus particles, 4) a separation region to isolate particles of different sizes, and 5) outlets to collect fractions of samples. By reducing the dimension of the channel cross section to 10 μm × 5.0 μm, the focusing phenomenon was observed for 0.92 μm PS particles (Fig. 2b). This study is significant as it enables the investigation of individual microorganisms and subcellular organelles at the downstream.

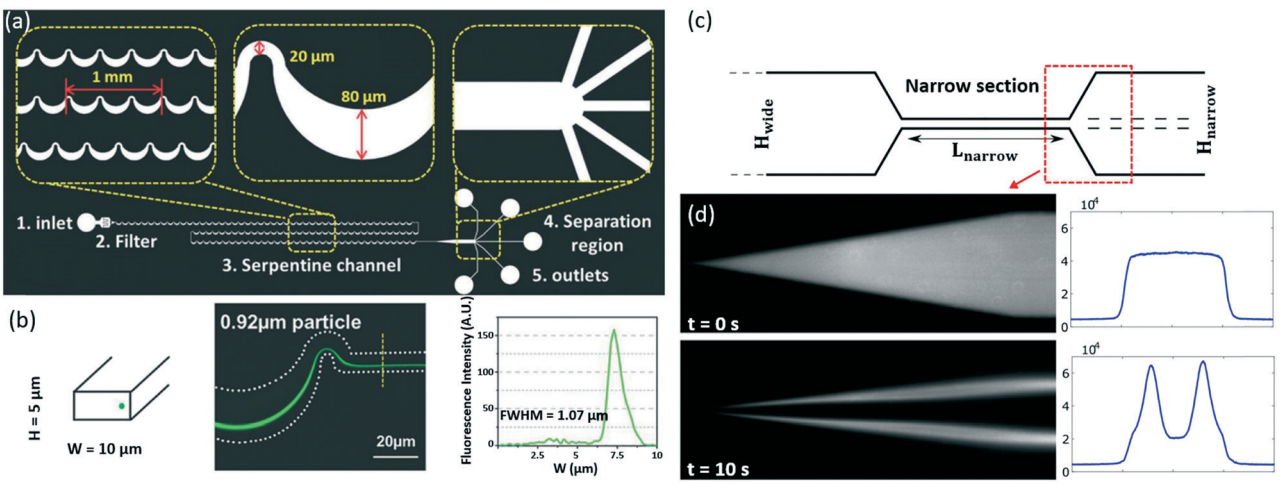

Fig. 2 Inertial focusing of sub-micrometer PS particles.[50,55] (a) Images showing the design of a serpentine microfluidic channel. Reproduced from ref. 50 with permission under open license CC BY 4.0. (b) The focusing of 0.92 μm PS particles (Green). Reproduced from ref. 50 with permission under open license CC BY 4.0. (c) A schematic of the bone-shaped microchannel (H_{narrow} = 10 μm, L_{narrow} = 250 μm, H_{wide} = 150 μm). Reproduced from ref. 55 with permission under open license CC BY-NC-ND 4.0. (d) Oscillatory inertial focusing of 0.50 μm PS particles. Both fluorescent streak images (left) and full-width half-maximum (FWHM) profiles (right) are presented to show the focusing performance. Reproduced from ref. 55 with permission under open license CC BY-NC-ND 4.0.

Besides a waved microchannel, a straight bone-like microchannel (Fig. 2c) was used by Mutlu *et al.* to focus PS particles as small as 0.50 μm (Fig. 2d) and round-shaped bacteria *S. aureus* with a nominal size of 0.80 μm.[55] In this design, the oscillatory microchannel switches the direction of the flow at a high frequency, but the force acting on the particles preserves its direction due to the symmetry of the velocity field along the flow axis. This allows indefinite extension of focusing length in theory, even though the channel has a short and fixed length. More recently, Cruz *et al.* investigated the mechanism of inertial focusing in curved channels for small (~1.0 μm) particles, and achieved the focusing of 0.50 μm PS particles.[56] This channel also realized size-based separation of sub-micrometer bacteria, *e.g.*, *Salmonella typhimurium* (*S. typhimurium*) and *Klebsiella pneumoniae* (*K. pneumoniae*) based on their difference in lateral equilibrium positions.

Using inertial microfluidics for the focusing of sub-micrometer particles is still challenging now, as it requires the increase in channel length and improvement in theory for effective focusing.[57] Inertial focusing shows the merits including high throughput, the simple sample preparation process, easy operation, no need for sheath flow, *etc.*, but it has its demerits, *e.g.*, the difficulty in improving focusing resolution.

2.2 Viscoelastic microfluidics

Viscoelastic focusing (Fig. 1b) takes advantage of three main hydrodynamic forces including inertial lift force (F_L, eqn (2)), elastic force (F_E, eqn (5)) and viscous drag force (F_D, eqn (6)) to focus particles to equilibrium positions in viscoelastic fluids, *e.g.*, dilute polymer solutions.[58] Inertial lift force, which is determined by the combination of shear gradient lift force and wall lift force, can be expressed as follows,[49,59]

$$F_L = \frac{\rho_f {v_m}^2 d^4}{{D_h}^2} f_L(R_c, x_c) \quad (2)$$

$$R_c = \frac{\rho_f v_m D_h}{\mu_f} \quad (3)$$

where ρ_f, μ_f and D_h are fluid density, dynamic viscosity and hydraulic diameter for the channel, and v_m, d and f_L (R_c, x_c) are maximum velocity of the channel flow, particle diameter and lift coefficient of net inertial lift force. R_c is Reynolds number. The particle influenced by elastic effects in viscoelastic fluids can be characterized by a dimensionless Weissenberg number W_i as below,[60]

$$W_i = \frac{\lambda}{t_f} = \lambda\dot{\gamma} = \lambda\frac{2v_m}{D_h} \quad (4)$$

where λ, t_f, and $\dot{\gamma}$ represent fluid relaxation time, characteristic time of the channel flow, and average (characteristic) shear rate, respectively. W_i denotes the ratio of elastic force, F_E, to viscous force.[61] When W_i is very small, F_E can be formulated as follows,[62]

$$F_E = -2C_{eL} d^3 \eta_p \lambda \nabla\dot{\gamma}^2 \quad (5)$$

where C_{eL}, η_p and ∇ respectively refer to non-dimensional elastic lift coefficient, polymeric contribution to solution viscosity and gradient operator. The relative importance of elastic to inertial effects can be defined as El, ratio of W_i to R_c (El = W_i/R_c). F_D arises from the difference between fluid element velocity (v_f) and particle velocity (v_p). Assuming that a spherical particle undergoes uniform Stokes flow, F_D can be expressed by the following formulation,[49,63]

$$F_D = 3\pi\mu_f d(v_f - v_p) \quad (6)$$

In viscoelastic fluids, the migration of particles can be described in viscoelasticity-dominant flow or elasto-inertial flow based on the relative importance of elastic and inertial effects.[62] Please refer to the review by Squires *et al.* to get an in-depth understanding of the dimensionless parameters such as R_c, W_i and Peclet (Pe).[64]

In 2012, Kim *et al.* found that PS particles as small as 0.20 μm can be focused at a flow rate of 15 μL h^{-1} under the effect of viscoelastic flows.[65] Besides, the focusing of flexible DNA molecules, including λ-DNA and T4-DNA with radii of gyration of around 0.69 μm and 1.50 μm, respectively, were observed to be enhanced using viscoelastic flows. This study lays the foundation for future development of viscoelastic focusing devices by demonstrating the importance of viscoelastic effects and the relative dimension of particle size to channel height. However, scaling the resolution down from micrometer to nanometer scale does not simply correspond to a scaling of dimensions, because new physics such as diffusion and particle–polymer interaction begin to dominate and need to be considered.[66]

By employing extensive computer simulations, Nikoubashman *et al.* revealed the focusing mechanism of colloidal particles in a viscoelastic fluid under Poiseuille flow and further exploited the mechanism to separate and capture sub-micrometer particles in simple microfluidic devices.[67] In 2014, Santo *et al.* developed a theory that can be applied to viscoelastic focusing of sub-micrometer particles, which was confirmed experimentally by focusing 0.20 μm PS particles.[68] This work links the particle trapping force caused by the viscoelasticity of the suspending fluid to a dimensionless parameter comparing viscoelasticity normal forces and Brownian forces. This theory can be used to downscale flow cytometers, and to guide the design of microfluidic devices for counting, coding and separating sub-micrometer and even nanometer particles. In addition to PS particles and DNA molecules, sub-micrometer *E. coli* was shown to be focused into a tight streamline by viscoelastic effects in straight microchannels.[69]

In 2016, Liu *et al.* achieved viscoelastic focusing of λ-DNA molecules, 0.10 μm PS particles and nanometer DNA origamis in a double spiral microchannel by systematically studying the effects of molecular weight, concentration of polymer, flow speed and particle size on the focusing performance.[70] In this study, aqueous solutions of polyethylene oxide (PEO) with low molecule weight (M_w of

0.60×10^6 g mol^{-1}) and low concentration (c of 0.60 wt%) were shown to be optimal for focusing 0.10 μm PS particles (Fig. 3a). Additionally, the focusing of DNA origami having three different shapes including spheres (0.04 μm in diameter), short tubes (0.03 μm in diameter and 0.04 μm in length) and long tubes (0.01 μm in diameter and 0.30 μm in length) were demonstrated (Fig. 3b). Liu *et al.* also demonstrated the selectively focusing and separation of a binary mixture of 0.10 and 0.50 μm PS particles by viscoelastic microfluidics in a straight microchannel,[71] where 0.50 μm PS particles were focused into the center of the microchannel, while 0.10 μm PS particles were deflected towards the sidewalls. Both of the particles were collected at the outlets with a recovery rate of over 90%. The same design was applied to separate exosomes ranging from 0.03 to 0.20 μm using PEO solutions of different concentrations.

More recently, Liu *et al.* reported a λ-DNA- and aptamer-mediated approach for the separation and detection of subpopulations of extracellular vesicles, including exosomes (0.03 to 0.2 μm), microvesicles (0.20 to 1.0 μm) and apoptotic bodies (>1.0 μm).[72] The focusing behaviors of PS particles with different sizes (*i.e.*, 0.10, 0.20, 0.30, 0.50 and 2.0 μm) and size-based particle separation were visualized, confirming the feasibility of separating extracellular vesicles subpopulations. Moreover, Zhou *et al.* realized the focusing of large extracellular vesicles ranging from 0.20 to 1.0 μm by a wavy channel using viscoelastic fluids (Fig. 3c). The focusing of 0.30 and 0.50 μm PS particles at different PEO concentrations (*e.g.*, 0.08%, 0.10%, 0.12%, 0.14% and 0.16%) was investigated (Fig. 3d) before running experiments with biological samples, which provides a foundation for the focusing and size-based sorting of large extracellular vesicles.[73]

With the improvement in theory and the optimization in experimental operating conditions, the resolution of viscoelastic particle focusing has advanced from micrometer to sub-micrometer and even nanometer scale. Viscoelastic focusing method is label-free, size-dependent and easy to operate, but the particle–particle interaction directly impairs the focusing performance. Thus, it is necessary to establish theoretical models and perform experiments to fully evaluate the effects of particle–particle interaction on viscoelastic microfluidics to improve the focusing performance.[62]

2.3 Deterministic lateral displacement (DLD)

DLD uses pillar arrays tilted with respect to the average flow direction to generate unique flow streamlines, which can be used for focusing particles in a size-dependent manner (Fig. 1c). For example, particles larger than the critical diameter (D_c, eqn (7)), usually considered to be the width of the first streamline, move forward in a bumping mode, while particles smaller than D_c go laterally in a zig-zag mode through the pillars. The bumping and zig-zag trajectories are considered as focusing streamlines. An equation expressing D_c of the DLD device is shown below,[74]

$$D_c = 1.4G\varepsilon^{0.48} \quad (7)$$

where G is device gap and ε is the slope of the pillar array ($\tan\theta = \varepsilon$), in which θ is the angle of the pillar array gradient.

In 2004, Huang *et al.* demonstrated that 0.80, 0.90 and 1.03 μm fluorescent particles can be focused and sorted continuously to different streamlines based on size at a flow rate of ~400 μm s^{-1}.[75] In this device, the D_c at the inlet was smaller (*i.e.*, <0.80 μm), so that all particles follow the displacement mode, but the gaps increased at the downstream, causing smaller particles to follow the zig-zag mode. This work showed that 0.80 μm particles quickly move in a zig-zag mode, while the 0.90 and 1.03 μm particles change their flow behaviors in the fourth and eighth

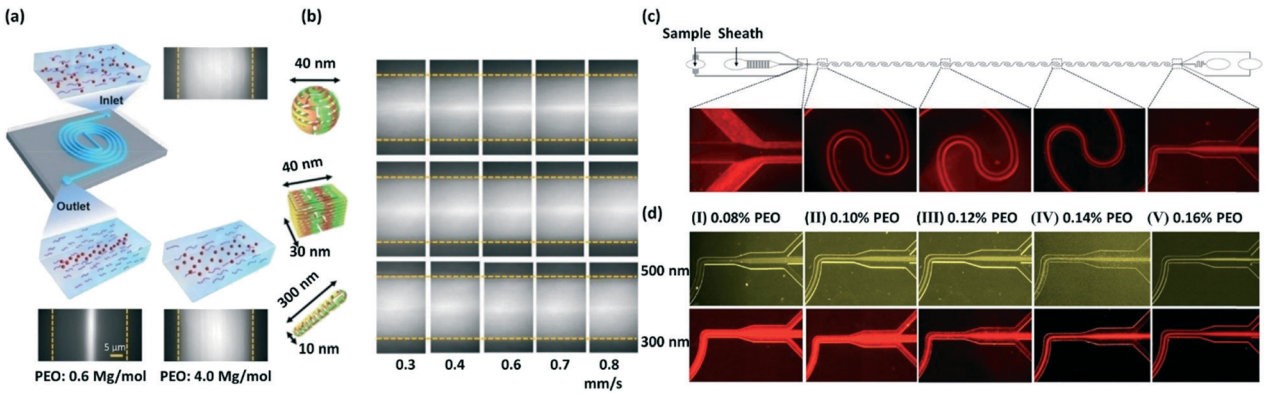

Fig. 3 Viscoelastic focusing of DNA origami structures,[70] large extracellular vesicles and sub-micrometer PS particles.[73] (a) Viscoelastic focusing of 0.10 μm PS particles in a double spiral microchannel using PEO solutions (not to scale). Reproduced from ref. 70. Copyright 2016, American Chemical Society. (b) Viscoelastic focusing of DNA origami with three different structures, *i.e.*, sphere, short and long tube in a waved microchannel using a PEO solution of $M_w = 0.60 \times 10^6$ g mol^{-1} and c = 1.80 wt%. Reproduced from ref. 70. Copyright 2016, American Chemical Society. (c) A schematic for the focusing of large extracellular vesicles ranging from 0.20 to 1.0 μm using viscoelastic fluids. Zoom-in experimental figures showing the lateral migration of large extracellular vesicles from sidewalls to the channel center. Reproduced from ref. 73. Copyright 2019, American Chemical Society. (d) The focusing of 0.30 and 0.50 μm PS particles at the trifurcated outlets using PEO solutions with five different concentrations of 0.08%, 0.10%, 0.12%, 0.14% and 0.16%. Reproduced from ref. 73. Copyright 2019, American Chemical Society.

sections, respectively. Further, the focusing and sorting of two bacterial artificial chromosome DNAs with 61 and 158 kb in size were demonstrated.

Advances in both theory and experimental conditions were increasingly seen in DLD, allowing shape-based focusing and separation of particles at sub-micrometer scale.[76] In 2014, Ranjan *et al.* found that spherical and non-spherical bioparticles can be focused to different tight streams using DLD, allowing the shape-based separation of sub-micrometer bioparticles.[77] More specifically, in the DLD device with an array of I-shaped pillars, non-spherical *E. coli* (~0.50 μm wide and ~2.0 μm long) mainly moved forward in a bumping mode from the inlet (Fig. 4a and b) to the outlet (Fig. 4b and c) while the spherical *S. epidermidis* (~0.70 μm in diameter) followed a different path, resulting in the separation by shape. Similarly, the non-spherical *K. pneumoniae* (~0.60 μm wide and ~1.80 μm long) and *Pseudomonas aeruginosa* (*P. aeruginosa*, ~0.60 μm wide and ~1.60 μm long) showed the similar focusing behaviors to non-spherical *E. coli*. However, focusing particles smaller than 0.50 μm was shown to be challenging at that stage, as the effects such as diffusion and electrostatic forces become significant for smaller particles.[78,79] In 2016, the focusing of PS particles as small as 0.051 μm was achieved using a DLD device with a large pore of 2.0 μm.[74] More importantly, the focusing and size-based separation of exosomes ranging from 0.02 to 0.14 μm has been demonstrated using a nanometer spherical DLD array (Fig. 4d), opening the door for on-chip sorting and quantification of significant biological particles.[80] Also, this work demonstrated the capability of fabricating DLD device with gaps as small as 0.025 μm (Fig. 4e). By adjusting the gap to 0.235 μm, Wunsch *et al.* demonstrated the focusing of 0.05 μm (yellow) and 0.11 μm (blue) PS particles in a pillar array (Fig. 4f). The detailed theories of DLD for nanometer particle focusing can be found in a study by Kim *et al.*,[81] where a unified theoretical framework to predict particle trajectories in the whole pillar arrays was presented. This theory can be used not only to explain the unexpected particle trajectories but also to design DLD arrays for small particle focusing. Predictions from the theoretical framework were validated experimentally by focusing 0.05 μm PS particles with carboxylate groups. This work provides guidelines for modifying the geometry of pillar arrays to tune the critical diameter as well as the migration of small particles in an altered zig-zag mode.

The resolution of DLD focusing has advanced from sub-micrometer scale to nanometer scale to date, enabling various biomedical and biological applications, *e.g.*, separation of exosomes. DLD focusing shows advantages such as label-free operation, easy operation, and high focusing resolution. Although the theories of DLD focusing are improved greatly, its implementation is limited to some extent by clogging induced by particle–particle or particle–surface interactions.[76] Anisotropic permeability, the microfluidic array's inherent tendency to induce an undesired lateral pressure gradient and unpredictable particle trajectories, becomes severe for arrays with unequal axial and lateral gaps or with highly asymmetric shapes.[82] Moreover, the fabrication process for DLD devices is quite complex.

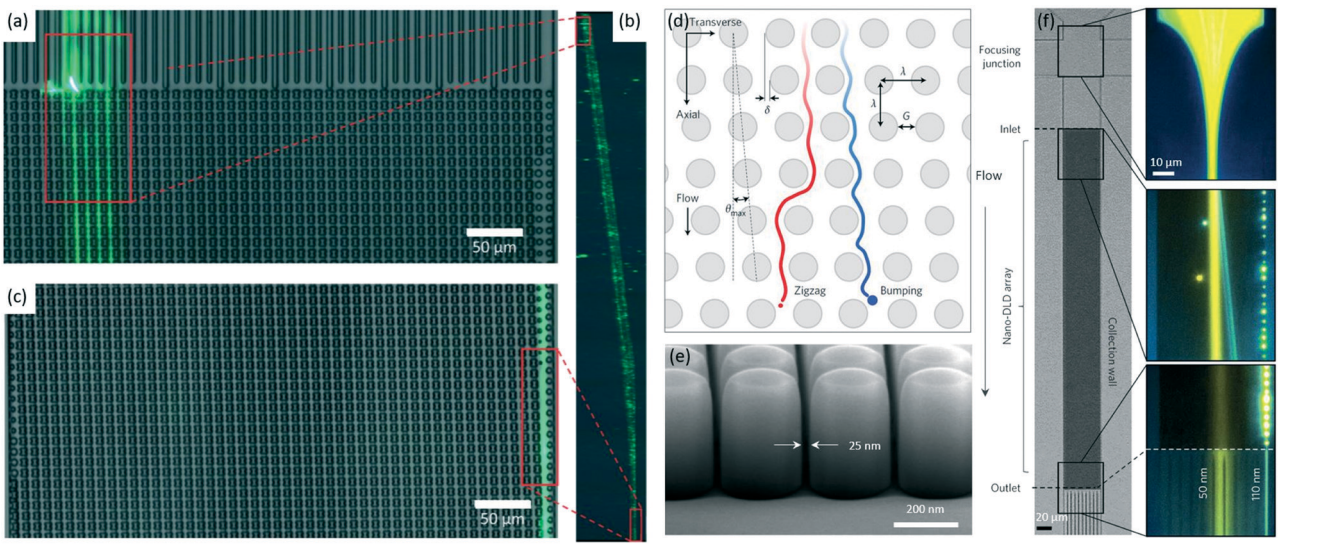

Fig. 4 Sub-micrometer particle focusing using DLD pillars with two different shapes: spherical and I-shaped.[77,80] (a–c) *E. coli* (green) in a DLD device with an array of I-shaped pillars mainly moves from the inlet (a) *via* a bumping mode (b) to the outlet (c). Reproduced from ref. 77 with permission from the Royal Society of Chemistry. (d) A schematic of a spherical pillar array. Particles with diameter D_P, below the critical diameter, D_C, follow a laminar flow in a zig-zag mode (red), whereas larger particles with $D_P \geq D_C$ follow maximum angle θ_{max} in a bumping mode (blue). Reproduced from ref. 80 with permission from Springer Nature. (e) A scanning electron microscope image of an array with λ = 400 nm and G = 25 nm. Reproduced from ref. 80 with permission from Springer Nature. (f) The focusing of 0.05 (right-most jet, blue) and 0.11 μm (left-most jet, yellow) PS particles in an array with a gap of 0.235 um. The initially injected mixture of particles splits into two streamlines due to their differences in lateral displacements. Reproduced from ref. 80 with permission from Springer Nature.

3. Active methods

Unlike passive techniques, active microfluidic techniques depend on the external fields to generate driving forces to direct sub-micrometer particles to their equilibrium focusing positions. This section discusses three main types of approaches including dielectrophoresis, acoustophoresis and thermophoresis, which use electric field, acoustic field and thermal field, respectively, to focus sub-micrometer particles.

3.1 Dielectrophoresis

Dielectrophoretic (DEP) focusing arises from the translational motion of particles by the forces exerted by a non-uniform electric field on the electric dipoles of particles (Fig. 1e). If there are electric field non-uniformities normal to streamlines, particles can be deflected across the streamlines by DEP force (F_{DEP}, eqn (8)), and finally focused to a tight streamline under the combined effect of DEP and hydrodynamic forces.[83,84] The magnitude and direction of F_{DEP} on a spherical particle depends on electric field strength (E), permittivity of particle and fluid, and Clausius–Mossotti factor (β), which are formulated as follows,[85]

$$F_{DEP} = 2\pi\varepsilon_m R^3 \,\mathrm{Re}(\beta)\nabla E^2 \quad (8)$$

$$\beta = \frac{\varepsilon_p^* - \varepsilon_m^*}{\varepsilon_p^* + \varepsilon_m^*} \quad (9)$$

where ε_m is medium permittivity and R is particle radius. $\varepsilon^* = \varepsilon - i\sigma/\omega$ represents effective complex permittivity, where ε, σ and ω are dielectric permittivity, electric conductivity and angular frequency of the applied electric field. Subscript "p" and "m" indicate the quantities for particle and medium, respectively. Particles will be repulsed to the lower electric field when the real component of the Clausius–Mossotti factor is greater than zero ($\mathrm{Re}(\beta) < 0$), and attracted to the higher electric field when $\mathrm{Re}(\beta) > 0$. Here, the attractive ($\mathrm{Re}(\beta) > 0$) and repulsive ($\mathrm{Re}(\beta) < 0$) processes are defined as positive and negative DEP focusing, respectively. In addition to metal-electrode based DEP (eDEP), insulator-based DEP (iDEP) also works for sub-micrometer particle focusing, where the non-uniform electric field is induced by insulating structures.[86]

In 2010, Kayani *et al.* designed a microfluidic device (Fig. 5a) with curved electrodes to focus smaller (<1.0 μm) particles (Fig. 5b and c).[87] Using deionized water with relative permittivity of 77.6 and electric conductivity of 2×10^{-4} S m^{-1}, as the suspending medium, the focusing of 0.23 μm silica particles into a single stream has been demonstrated (Fig. 5d) at a flow rate of 10 μL min^{-1} (the magnitude and frequency of the alternating current, AC, field is 15 V and 5.0 MHz, respectively). Similarly, a narrow focal stream was observed for 0.45 μm silica particles at a flow rate of 2.0 μL min^{-1} (Fig. 5e). Further, Chrimes *et al.* demonstrated the focusing of

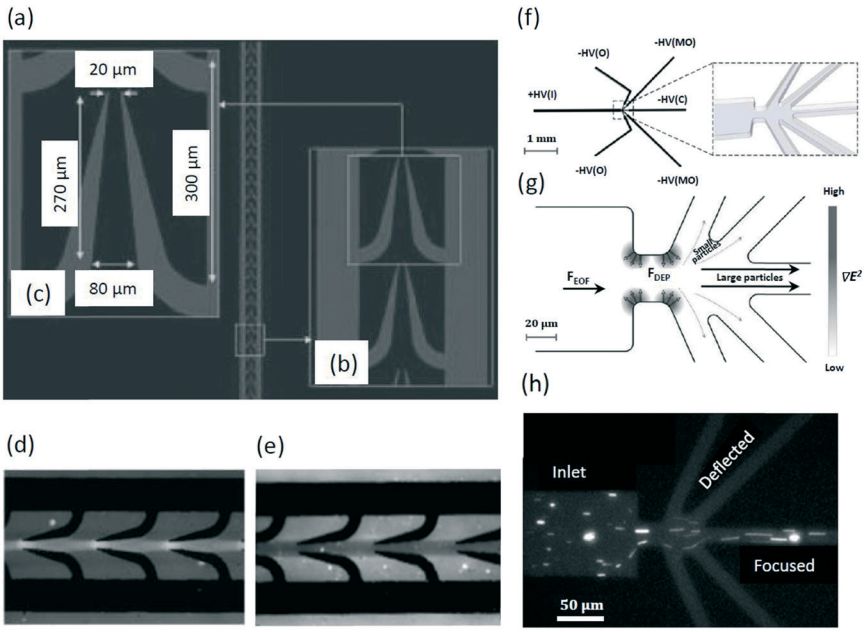

Fig. 5 DEP devices for the focusing of silica particles[87] and PSI crystals.[26] (a) A DEP electrode array consists (b) curved electrodes with (c) specific dimensions. Reproduced from ref. 87 with permission from John Wiley and Sons. DEP focusing of (d) 0.23 and (e) 0.45 μm silica particles. Reproduced from ref. 87 with permission from John Wiley and Sons. (f) A schematic of the entire iDEP focusing and sorting device (without reservoirs for clarity). The zoom-in schematic shows the constriction region connecting the inlet channel to the outlets (right). Reproduced from ref. 26. Copyright 2013, American Chemical Society. (g) Larger particles are focused toward the center of the device while the smaller particles are deflected into the side outlet channels using iDEP. Reproduced from ref. 26. Copyright 2013, American Chemical Society. (h) A fluorescent image of PSI crystal focusing. Reproduced from ref. 26. Copyright 2013, American Chemical Society.

~0.22 μm PS particles and ~0.08 μm tungsten trioxide (WO_3) particles using a similar electrode design.[88] A study by Park *et al.* demonstrated the focusing of *E. coli* by negative DEP at the upstream channel, which facilitates the separation from blood cells by positive DEP at the downstream.[89]

In 2013, an simulation of iDEP by Abdallah *et al.* showed the separation of 0.09 μm particles from 0.90 μm ones by focusing the larger particles in the center while deflecting the smaller ones to the side channels.[26] The microfluidic device consists of one inlet for sample injection, where positive potential is applied, and five outlets with negative potentials for the collection of the sorted fractions (Fig. 5f). The inlet channel and outlet channels are connected by a constriction region, which is used to produce an inhomogeneous electric field (Fig. 5f, right). When flowing from the inlet to outlets driven by electroosmosis, larger particles are focused to the channel centerline by negative DEP force (Fig. 5g). Based on this mechanism, larger photosystem I (PSI) crystals were focused into the center of the microchannel, while the smaller ones of around 0.10 μm were deflected to the outlets closer to the sidewalls (Fig. 5h).

Kim *et al.* reported that *E. coli* can be focused under high flow rate conditions (*e.g.*, 25 μL min^{-1}) using positive DEP.[90] The focused *E. coli* can be captured by the electrodes to serve as sensors, showing the potential for the development of portable and highly sensitive chips that can enable rapid detection of bacteria in drinking water. In 2017, the focusing of λ-DNA of 48.5 kb was achieved, along with its separation from plasmid DNA of 10.2 kb.[91] Interestingly, Rozynek *et al.* showed that conductive particles with diameters ranging from sub-micrometer to micrometer scale could be focused using DEP forces and then deposited onto the surface of any materials, *e.g.*, glass, to form desired conductive patterns, holding promise for the manufacturing of circuits.[92] By combining with accurate control over the conductivity of sub-micrometer particles, it may allow the use of microfluidics for precise particle patterning.

Although DEP focusing shows advantages such as high focusing resolution, real-time control, *etc.*, it is still limited to the complicated process for sample preparation and the risk of sample damage. The main demerit of DEP is the demand for the sample with low conductivity, such as deionized water and sucrose solution.[93,94] Unfortunately, most clinical samples and food matrices, *e.g.*, whole human blood and cow's milk, have high conductivity,[95,96] making them unsuitable for use in DEP devices. In summary, as one of the main pillars of particle manipulation techniques in microfluidics, DEP is widely used and still catching interests in the future.[97–100]

3.2 Acoustophoresis

Acoustophoretic focusing refers to the use of acoustic waves to induce particle lateral migration towards or away from pressure nodes or antinodes (Fig. 1f). It depends not only on the density and compressibility of the suspending medium but also on the size, density and compressibility of the particle. There are two types of acoustic standing waves: 1) bulk acoustic waves operating at the frequency usually in the range from 1.0 to 10 MHz, and 2) surface acoustic waves (SAWs) which can be further classified into traveling surface acoustic waves (TSAWs) and standing surface acoustic waves (SSAWs).[101,102] Since the acoustic force is proportional to the SAW frequency, higher operating frequency (*e.g.*, 636 MHz) is always used to counterbalance the drag force to focus particles smaller than 1.0 μm.[103–106] A TSAW arises from an AC signal applied to interdigitated transducers (IDTs) on piezoelectric substrates, while an SSAW arises when two TSAWs interfere oppositely.[102,107] In an SSAW, the acoustic force (F_a) can be calculated by the acoustic pressure (p) on a spherical particle with d in diameter as below,[28,108]

$$F_a = \frac{\pi^2 p^2 d^3}{12\lambda}\beta_m \phi \sin\left(\frac{4\pi}{\lambda}y\right) \quad (10)$$

$$\phi = \frac{\left(5\rho_p - 2\rho_m\right)}{\left(2\rho_p - \rho_m\right)} - \left(\frac{\beta_p}{\beta_m}\right) \quad (11)$$

where β_m and β_p are compressibility of medium and particle, respectively, ρ_m and ρ_p are density of medium and particle, respectively, ϕ is acoustic constant factor, y is the distance from a pressure node and λ is ultrasonic wavelength. When SSAWs encounter the liquid medium inside the channel, leakage waves in the longitudinal mode are induced, resulting in pressure fluctuations in the medium.[109] These pressure fluctuations induce acoustic radiation forces acting laterally on the particles. Then, the suspended particles will be directed toward either the pressure nodes or antinodes, depending on the density and compressibility of the medium and suspending particles, as well as the size of particles (eqn (10) and (11)).

Using SSAW-induced acoustophoresis, it demonstrated that 0.87 μm PS particles can be focused along the sidewalls of the microchannel at flow rates ranging from 0.60 to 2.0 μL min^{-1}.[108] Continuous particle separation and a subsequent collection at the downstream have been achieved. Also, 0.50 μm PS particles are steadily aligned into a focal streamline by SAWs at a flow rate of 0.20 μL min^{-1}.[101] In 2014, Destgeer *et al.* designed a cross type particle sorter that could generate TSAWs by a focused IDT (Fig. 6a).[102] This device enabled the separation of 0.71 and 3.0 μm PS particles by focusing them into different streamlines by TSAWs at 200 MHz (Fig. 6b). Also, a study by Collins *et al.* showed that 0.50 μm PS particles can be focused using SAWs.[110] By taking advantage of the acoustic streaming induced drag force, Antfolk *et al.* achieved the focusing of *E. coli* and PS particles as small as 0.50 μm with a recovery rate of over 90% using bulk acoustic waves.[27]

In 2015, Lee *et al.* showed that exosomes are able to be focused using acoustic forces in an SSAW-based device,[28] which consists of a pair of IDT electrodes to produce SSAWs across the flow, and two side outlets and one center outlet for collecting larger extracellular vesicles and exosomes,

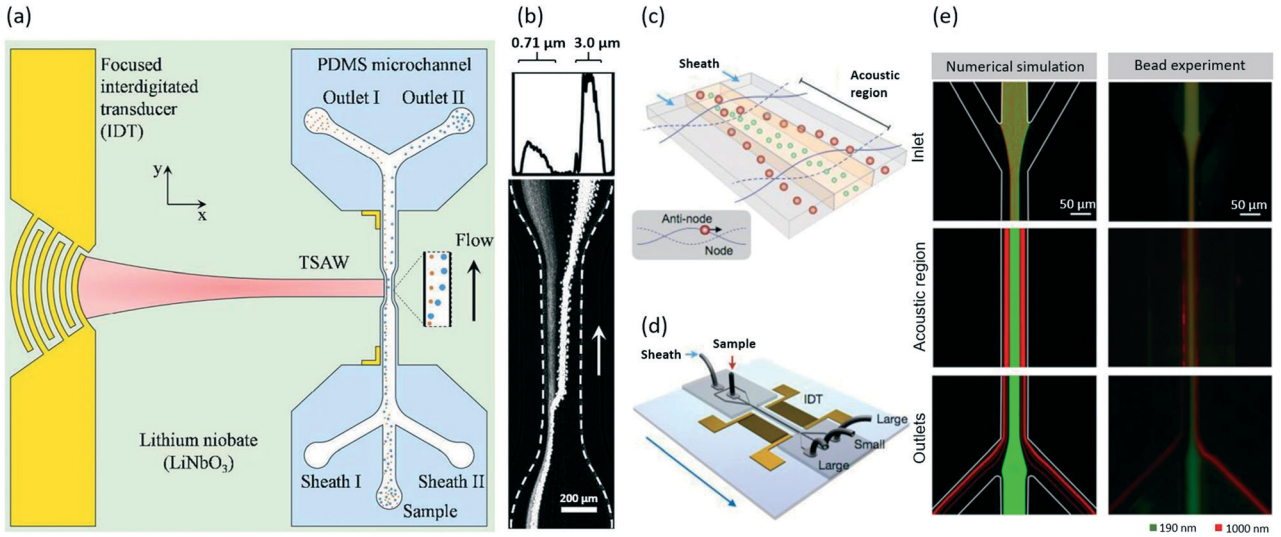

Fig. 6 Acoustic focusing of PS particles[102] and extracellular vesicles.[28] (a) A schematic showing the cross type acoustic particle separator. The TSAWs generated by the IDT are coupled with the fluid inside the PDMS microchannel. The particles are collected at separate outlets. Reproduced from ref. 102 with permission from the Royal Society of Chemistry. (b) The focusing of 0.71 and 3.0 μm PS particles into different streamlines with TSAWs. The plot (top) shows the scattering light intensity from the particles across the width of the microchannel. Reproduced from ref. 102 with permission from the Royal Society of Chemistry. Schematics of (c) the operation mechanism with SSAWs and (d) the acoustic device. Reproduced from ref. 28. Copyright 2015, American Chemical Society. (e) Numerical and experimental results showing the focusing of 0.19 μm (green) and 1.0 μm (red) PS particles to focal streamlines at different lateral positions using SSAWs. Reproduced from ref. 28. Copyright 2015, American Chemical Society.

respectively (Fig. 6c and d). They also demonstrated the focusing of 0.19 and 1.0 μm PS particles in both numerical simulations and experiments (Fig. 6e). Then this device was utilized for selective isolation of exosomes smaller than 0.20 μm by displacing the larger extracellular vesicles to nodes of acoustic pressure region (Fig. 6c). During this process, the larger extracellular vesicles move faster compared to smaller ones due to larger acoustic force that is proportional to the volume of extracellular vesicles.

In 2018, Gautam *et al.* reported the use of SAWs for focusing *E. coli* and 0.25 μm PS particles by displacing them to different lateral positions within the microchannel.[111] This work is important as it achieves high-speed (50 μL min^{-1}) separation of micrometer and sub-micrometer particles by displacing particles to different size-dependent streamlines. Also, the focusing of *E. coli* was demonstrated using tilted-angle SSAWs.[112] More recently, Wu *et al.* achieved the focusing of extracellular vesicles and lipoproteins using SSAWs, leading to continuous particle separation at the downstream.[113] Please note that these two types of sub-micrometer particles are similar in size, but their acoustic properties, the tendency to move to the nodes or antinodes, are different.

Acoustophoretic focusing is potentially useful for health monitoring, disease diagnosis and personalized medicine. It shows merits such as non-contact, gentle and label-free manipulation, making it as a promising technique for sub-micrometer particle focusing. Although inherently limited by the attenuation of acoustic waves, the understanding of acoustic focusing in fluids has greatly advanced in parallel with development in devices and fundamentals of piezoelectricity, piezoelectric materials and transducers.[114]

3.3 Thermophoresis

Thermophoresis is a process in which suspended particles are driven towards the lower temperature region in non-isothermal mixtures. Thermophoretic focusing refers to the focusing of particles by adjusting thermophoretic force (F_T) acting on the suspended particles when a temperature gradient exists (Fig. 1g). For example, the particles can be equilibrated to the isothermal layer due to F_T (eqn (12)) within a channel. After the discovery of thermophoretic phenomenon by Maxwell, Epstein quantitated F_T on a spherical particle in a gas by an equation, which was further improved by Brock and Talbot *et al.* for more general predictions.[115–117] F_T can be expressed as below,[118]

$$F_T = \frac{6\pi\mu_f^2 d_p}{\rho_f} C_s \frac{k_f}{k_p + 2k_f} \frac{\nabla T}{T_f} \quad (12)$$

where μ_f is dynamic viscosity of the fluid, d_p is particle diameter, ρ_f is fluid density, C_s equals 0.13 for particles on the order of 1.0 μm,[119] k_f is fluid thermal conductivity, k_p is particle thermal conductivity, ∇T is uniform temperature gradient and T_f is fluid absolute temperature.

Thermophoretic behavior is similar to that of thermodiffusion as the size of the suspended phase is similar to the one of the molecules, indicating the key role of thermophoretic force on the particles with the size in the range of 0.10 to 1.0 μm.[120] The simulation by Eslamian *et al.* demonstrated that 1.0 μm gold particles can be focused to a streamline close to channel center within a channel having a 20 K difference in temperature between the channel walls (a velocity of 50 mm s^{-1}).[121] By using a similar microchannel

(Fig. 7a), the focusing of sub-micrometer particles ranging from 0.10 μm to 1.0 μm was achieved by thermophoretic effects.[118] The numerical simulations in this work showed that 0.10, 0.50 and 1.0 μm particles can be focused to different lateral positions when there is a 10 K temperature difference between channel walls. Here, the velocity gradient across the width of the channel is almost constant (Fig. 7b), while the temperature gradient across the channel width shows a dramatic decrease, enabling the thermophoretic force to drive relatively larger particles upwards by counterbalancing the gravitational force (Fig. 7c). When the temperature difference between channel walls was changed to 2.0 K, it showed that 0.50 μm particles that randomly distributed at the inlet (Fig. 7d) can be focused at 3.0 mm downstream (Fig. 7e). It should be noted that both numerical simulations and experiments have been performed to demonstrate the successful focusing of sub-micrometer particles by thermophoresis. Thermophoretic focusing of sub-micrometer charged PS particles was also observed in experiment.[122] Zhou *et al.* demonstrated that 0.74 μm charged PS particles can be focused and then sorted from the 2.0 μm ones in a size-dependent manner using thermophoresis.

Based on the information provided above, we can see that the resolution in thermophoretic focusing has improved, indicating the potential of further applications in the detection and separation of nanometer particles in a label-free manner. However, thermophoresis may induce thermophysical changes in bioparticles, *e.g.*, lipid vesicles.[123]

4. Other methods

Besides the six main microfluidic methods discussed above, there are a few more techniques applicable for sub-micrometer particle focusing, such as hydrophoresis, optical tweezers, magnetophoresis and electrophoresis. Hydrophoretic and optical methods have been demonstrated for focusing particles at sub-micrometer scale, however, we failed to find any reports on sub-micrometer particle focusing by either magnetophoresis or electrophoresis.

Hydrophoresis refers to the movement of suspended particles using rotational flows induced by anisotropic obstacles (Fig. 1d).[124] Geometric parameters such as channel width and oblique angle of grooves can affect focusing efficiency.[125] By using anisotropic obstacles, 0.52 μm PS particles were shown to be focused by hydrophoretic effects at a flow rate of 5.1 mm s^{-1}.[124] The same device was also used for the separation of DNA molecules of 49 and 115 kb. Hydrophoresis is simple to operate, but it subjects to high probability of clogging since the obstacle height needs to be comparable to the particle size.[2]

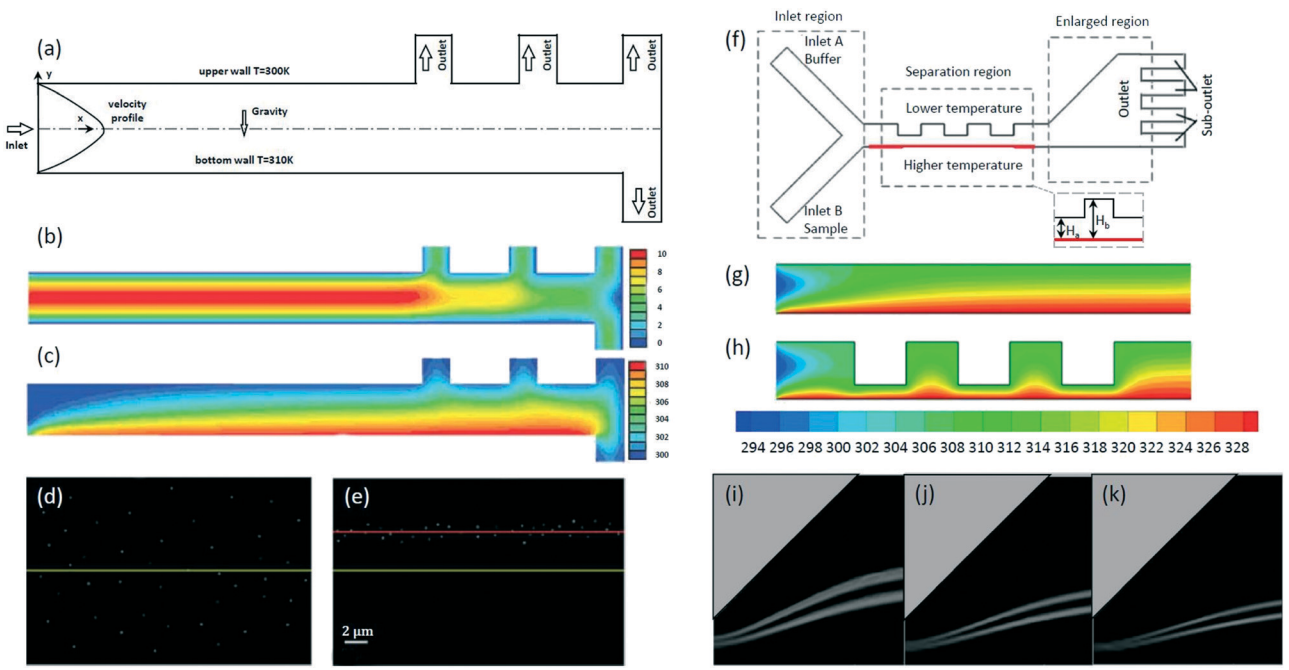

Fig. 7 The focusing of sub-micrometer particles using thermophoretic effects.[118,140] (a) The microchannel with a temperature difference between sidewalls for thermophoretic focusing of sub-micrometer particles. Reproduced from ref. 118 with permission from Taylor & Francis. Simulation results of (b) velocity contours and (c) temperature contours in the microchannel. Reproduced from ref. 118 with permission from Taylor & Francis. Experimental results showing that 0.50 μm PS particles are randomly distributed at the inlet (d) but focused at 3.0 mm downstream (e). The yellow and red lines represent the center of the channel and the particle focusing streamlines, respectively. Reproduced from ref. 118 with permission from Taylor & Francis. (f) A schematic of the thermophoretic sorter with an expansion–contraction microchannel. Simulation results of temperature gradient contours with an expansion–contraction ratio of (g) $H_b:H_a$ = 1 and (h) $H_b:H_a$ = 4. Reproduced from ref. 140. Copyright 2019, Elsevier. Experimental results showing the focusing of 0.50 μm (up) and 1.0 μm (low) fluorescent particles at the inlet velocity ratio of (i) $u_A:u_B$ = 4, (j) $u_A:u_B$ = 8 and (k) $u_A:u_B$ = 12. Reproduced from ref. 140. Copyright 2019, Elsevier.

Optical forces can be used to manipulate particles with size ranging from tens of nanometers to tens of micrometers.[126,127] The underlying mechanism of the optical focusing technique is identical to that of optical tweezers for particle trapping (Fig. 1h). Zhao *et al.* provided a method based on optical gradient forces to guide and focus particles in fluid flows by numerical simulations and particles as small as 0.10 μm were focused close to the center of the microchannel.[128] This method features non-contact, easy fabrication and operation, but it is limited by low flow rates (*e.g.*, 1.0 mm s^{-1}).

Magnetophoresis demonstrates its capability for the focusing of particles at micrometer scale, *e.g.*, superparamagnetic and diamagnetic particles and cells,[129–132] where the forces exerted on the particles are generated due to the difference in permeability between particles and the suspending medium. Electrophoresis, in which a uniform electric field is applied, enables the focusing of charged particles with different sizes into different streamlines in a size-dependent manner, and facilitates downstream separation in microfluidics.[133] A study by Kawamata *et al.* demonstrated that 1.0 and 2.1 μm particles are focused into different streamlines by electrophoretic forces.[134] Compared with DEP, electrophoresis is limited to charged particles.

Hybrid methods, which normally combine active and passive techniques, are emerging techniques that feature better performance in terms of stability, versatility and convenience.[135,136] The integration of 1) DLD with DEP, and 2) inertial microfluidics with thermophoresis have been demonstrated for the focusing of sub-micrometer particles. By introducing an electric field to DLD, the focusing of PS particles and extracellular vesicles was achieved in a tunable manner.[137,138] The integration of DEP with DLD can decrease the critical size of a DLD chip in a controlled manner, enabling the focusing not only depends on size but also on dielectric properties of target particles.[139] Also, this hybrid method shows other benefits, such as the decrease in the probability of clogging, as the D_c can be decreased with the aid of DEP without the need to reduce the size of the gaps between the pillars.

The integration of inertial microfluidics and thermophoresis enables the focusing of sub-micrometer particles at a relatively low flow rate.[140] Wang *et al.* achieved the thermophoretic sorting of 0.50 and 1.0 μm fluorescent particles by focusing them into different streamlines in an expansion–contraction microchannel with the aid of inertial microfluidics (Fig. 7f). Numerical simulations demonstrated that the contraction region with an expansion–contraction ratio of 4 (Fig. 7h) enhances the temperature gradient compared to the one with an expansion–contraction ratio of 1 (Fig. 7g). The enhanced temperature gradient increases the magnitude of the thermophoretic force exerted on particles, leading to the better focusing performance in the expansion region. Experimental results showed that 0.50 and 1.0 μm fluorescent particles were focused to upper and lower streamlines, respectively (Fig. 7i–k) at different inlet velocity ratios (ΔT = 5.0 K, u_B = 2.0 mm s^{-1}, $H_b:H_a$ = 4). Hybrid methods seem to be more promising for particle focusing as the research is becoming increasingly interdisciplinary.

5. Discussion

Microfluidics is capable of focusing sub-micrometer particles, such as PS beads, bacteria, exosomes and DNA, which are significant in biomedical, environmental and industrial fields. A variety of microfluidic techniques have been demonstrated for particle focusing with resolution at sub-micrometer scale, although it is still challenging for a couple of techniques such as hydrophoresis and inertial microfluidics to focus the particles as small as 0.10 μm. New physics begin to emerge and need to be considered as particle size decreases to sub-micrometer scale. In this section, we firstly talk about four types of particles within sub-micrometer range, and then the challenges including diffusion, throughput and resolution are discussed. We also talk about the ability of each method to integrate with downstream separation components. Lastly, design guidelines for the focusing of sub-micrometer particles using each technique are presented, which are expected to be useful for lab-on-a-chip researchers in both academia and industry.

5.1 Sub-micrometer particles

Polystyrene particles. Sub-micrometer PS particles are regarded as suitable model particles in research activities such as diagnosis, imaging and optical tracking,[45] because there are biocompatible, do not degrade in cellular environment and can be synthesized in a wide range of sizes. Most of the microfluidic techniques discussed in this review are applicable to the focusing of sub-micrometer PS particles.

Inertial microfluidics and hydrophoresis do not show high focusing resolution, as it calls for a significant increase in minimum channel length for inertial focusing and comparable obstacle height to particle size for hydrophoresis. DLD shows better performance in precise particle focusing and separation, especially for nanometer PS particles, but the throughput is quite low (*e.g.*, 0.05 μL min^{-1}),[74] which may limit its applications. Acoustophoresis is promising for the focusing of PS particles at sub-micrometer scale due to its high compatibility and advances in piezoelectric thin films.[141]

Bacteria. Sub-micrometer bacteria with at least one dimension less than 1.0 μm are of great significance to study. For example, *E. coli*, *K. pneumoniae* and *P. aeruginosa* are clinically relevant, and *E. coli* exists widely in humans, animals, food and environment.[142] The focusing of *E. coli* can be achieved using inertial microfluidics, viscoelastic microfluidics, DLD, DEP and acoustophoresis. Inertial microfluidics may be the most promising technique due to its features of high throughput and simple operation. Acoustophoresis can confine bacteria in a tight streamline at

a relatively low flow rate by structural improvements, *e.g.*, the use of 2D bulk acoustic waves[27] and an ultra-thin glass chip.[143] The throughput of viscoelastic microfluidics and DEP is not as high as that of inertial focusing.

DLD device with I-shaped pillars realizes the shape-based focusing and separation of the bacteria, by focusing the spherical *S. epidermidis* into the streamlines different to that of the rod-shaped bacteria including *E. coli*, *K. pneumoniae* and *P. aeruginosa*.[77] Although inertial microfluidics has been demonstrated for focusing of particles at micrometer scale by shape,[144,145] there is no report on sub-micrometer particles yet. Please note that other methods such as magnetophophoresis[146] and nanofluidics[147] have been demonstrated for the separation of bacteria.

Exosomes. Exosomes are lipid-bilayer-enclosed extracellular vesicles containing proteins and nucleic acids, which are released into extracellular space and enter the circulation.[148–150] Initially, its size range was defined as from 0.05 to 0.10 μm, then the range was increased to include those with size as small as 0.02 μm and over 0.10 μm (*e.g.*, 0.15 μm).[151,152] Although the strict definition by size or biogenesis has not been established yet,[153] numerous studies have focused on this type of extracellular vesicles due to their significant roles in intercellular communication,[154] drug delivery,[155] disease diagnostics,[151] *etc.* Acoustophoresis is commonly used for extracellular vesicles focusing and sorting in microfluidics, and shows high compatibility with other microfluidic components. It is capable for acoustic focusing of extracellular vesicles ranging from 0.10 to 1.0 μm.[156] However, when it goes down to the minimum exosome size (*i.e.*, 0.02 μm), this method becomes less effective, as both exosomes and smaller particles are focused in the same streamline. This drawback is also seen in viscoelastic microfluidics. DLD device shows great promise for exosome analysis with high precision, and the separation of 0.02 μm exosomes and smaller ones using DLD pillars has been demonstrated.[80] More recently, precise focusing of exosomes (0.05 to 0.20 μm) using electroosmotic flow-driven DLD was achieved.[137] Please note that exosomes may bump into smaller particles during the operation process. Therefore, it calls for attention to device design and flow rate selection. Also, the issues such as scalability, validation and standardization remain to be solved to allow a practical clinical applications for exosome diagnosis.[157]

DNA. DNA has a size ranging from nanometer to micrometer, and can construct complex topologies and secondary structures.[158] Microfluidic devices achieved direct observation and manipulation of DNA, enabling us to elucidate the relationship between the polymer microstructure and its rheological properties and to design new platforms for applications in biophysics and biomedicine.[159] Conventionally, gel electrophoresis is used for DNA separation, but it is time consuming and the process is very complicated.[160] The focusing of λ-DNA, T4-DNA and DNA origami using viscoelastic microfluidics facilitates the separation at the downstream.[65,70] The focusing of bacterial artificial chromosome DNAs with 61 and 158 kb was realized using DLD pillars in 2004.[75] Besides, DEP achieves size-based separation of DNA fragments (*e.g.*, 2.686 and 6.0 kb) by focusing different sized DNA fragments into different streamlines.[161] Both viscoelastic microfluidics and DLD demonstrated the ability to focus larger DNA particles, but DLD seems to be more promising for focusing DNA with smaller sizes in microfluidics.

5.2 Challenges

Diffusion. Diffusion is a physical process where a concentrated group of particles in a volume spread out over time by Brownian motion. Peclet (Pe) is used to describe the time to move a certain distance by radial diffusion and axial convection, which is formulated as below,[64]

$$\mathrm{Pe} \equiv \frac{vw}{D} = \frac{\text{diffusion time}}{\text{convection time}} \tag{13}$$

where v, w and D are flow velocity, microchannel width and diffusion coefficient, respectively. For micrometer-sized particles, the influences of diffusion are usually negligible. However, diffusivity is increasingly dominant as particle size decreases. For example, the particle trajectory in DLD devices is increasingly influenced by diffusion with the decrease in particle size.[76] It is possible to alleviate diffusion by improving flow velocity, but high velocity may make the fluid flow unstable in DLD devices. High flow velocity in inertial microfluidics helps focus sub-micrometer particles and reduce diffusion effects as well. The viscoelastic properties of suspending medium in viscoelastic microfluidics can make diffusion less obvious, hence, improving particle focusing efficiency. Active methods such as DEP, acoustophoresis and optical microfluidics also suffer from diffusion. Although the flow rates are relatively lower in these active techniques than those in inertial microfluidics, external forces generated by these techniques dominate over the influence of diffusion on target particles at sub-micrometer scale, which may make the focusing less affected by diffusion.

Throughput. Throughput plays an important role in widening the range of applications of focusing techniques, for example, practical and industrial applications require high throughput. When particles scale down to sub-micrometer, the dimensions of cross channel are always reduced for effective focusing, making fluidic resistance increasingly obvious and limiting the improvement in throughput. The fluid flowing in a channel subjects to an increase of fluidic resistance as channel dimensions decrease gradually because of the friction between channel walls and the fluid body.[76] Increasing the ratio of surface to volume usually results in an increase in fluidic resistance. The relationship between flow rate (Q) within a microchannel, pressure difference along the channel (ΔP) and channel resistance (R) is given as follows,[162]

$$Q = \frac{\Delta P}{R} \tag{14}$$

A common strategy to focus small particles is to scale down the channel dimensions. This usually works for passive methods due to their dependence on the intrinsic properties of fluids and channel geometry. For example, the downscaling of channel cross section contributes to the focusing of 0.92 μm PS particles at a flow rate of 500 μL min^{-1}.[50] The throughput of viscoelastic microfluidics is generally lower than that of inertial microfluidics, as the viscoelastic medium causes an increase in fluidic resistance. The ratio of surface to volume is relatively high for the fluid flowing in a DLD device, thus increasing fluidic resistance and contributing to the extremely low throughput. For example, a study by Wunsch *et al.* showed that the flow rate used for the focusing of exosomes (0.02 to 0.14 μm) ranges from 0.1 to 0.2 nL min^{-1}.[80] Besides, ΔP will increase with the increase of surface to volume ratio, resulting in a higher risk of device damage. Anisotropic obstacles are employed in hydrophoresis to induce rotational flows to arrange particles, leading to a relatively high ratio of surface to volume. Thus, the resultant fluidic resistance is high, which may be a reason for low throughput in hydrophoretic focusing of sub-micrometer PS particles.[124]

Active methods also encounter fluidic resistance with respect to the focusing of sub-micrometer particles. Further, particle focusing is influenced by the combined effects of hydrodynamic forces and driving forces enabled by external fields, thus the throughput cannot increase unlimitedly. Kim *et al.* achieved the focusing of *E. coli* using DEP at a moderate flow rate (25 μL min^{-1}),[90] which is similar to the flow rate used in thermophoresis (24 μL min^{-1}).[118] The flow rate applied in acoustophoresis (0.20 to 2.0 μL min^{-1}) is not high in the focusing of sub-micrometer PS particles,[27,101,102,108,110] except the one used by Gautam *et al.* (50 μL min^{-1}).[111] Although optical focusing of 0.10 μm particles has been achieved, the throughput is extremely low (0.24 nL min^{-1}).[128]

Resolution. Improvement of the size resolution of focused particles is also a challenge toward broadening applications of the field. It is still difficult to focus particles smaller than 0.50 μm for the passive methods such as inertial focusing[55,56] and hydrophoresis.[124] Although inertial focusing features relatively higher throughput, it calls for smaller channel cross sections and larger velocities to focus smaller particles. Viscoelastic microfluidics can achieve the focusing of sub-micrometer particles in 0.10 to 1.0 μm range, however, it is not able to purely focus exosomes ranging from 0.03 to 0.20 μm, since particles smaller than 0.03 μm are also forced to the same focal streamline.[72] DLD is capable of focusing particles as small as 0.02 μm, allowing the separation of exosomes ranging from 0.02 to 0.14 μm.[80] Also, its selective focusing allows continuous separation of 0.051 and 0.191 μm particles by size.[74] DEP shows to be capable of focusing 0.08 μm particles,[88] however, the requirement for samples with low conductivities[93,94] restricts its applications. Acoustophoresis is a mature technique that has been widely used for various applications, such as the separation of exosomes and other larger extracellular vesicles by focusing them to different streamlines.[163] Thermophoresis and optical focusing have been demonstrated for focusing 0.10 μm particles,[118,128] and more studies are needed to widen the sample types and potential applications. More importantly, it calls for further development in theory and practice to enable the applications for particles at nanometer scale.

5.3 Capability of integration with downstream separation components

Various microfluidic focusing techniques, such as inertial microfluidics,[164] DLD,[165] hydrodynamic sheath focusing,[166,167] DEP[168] and acoustophoresis[169,170] have demonstrated the capability of integrating with downstream sorting components for the separation of micrometer scale particles (*e.g.*, circulating tumor cells, microalgae cells, and PS particles). Unfortunately, there are only a few reports on the integration of upstream focusing with downstream sorting for applications to sub-micrometer particles. The challenges, such as fluidic resistance, diffusion and detection, may be accountable for this.

Hydrodynamic sheath focusing has been integrated with optical tweezers for the separation of sub-micrometer microbial cells.[171] In 2017, Wu *et al.* realized the separation of exosomes directly from whole blood using a microfluidic device with two sets of acoustic units (Fig. 8).[163] The upstream unit is responsible for the focusing of apoptotic bodies, exosomes and microvesicles while deflecting larger particles including white blood cells, red blood cells and platelets. Then, the downstream unit achieves the separation of exosomes, apoptotic bodies and microvesicles (Fig. 8a and b). Larger particles are subjected to a larger acoustic force enabled by the SAW field, and are driven toward the pressure node (Fig. 8c). This work demonstrates

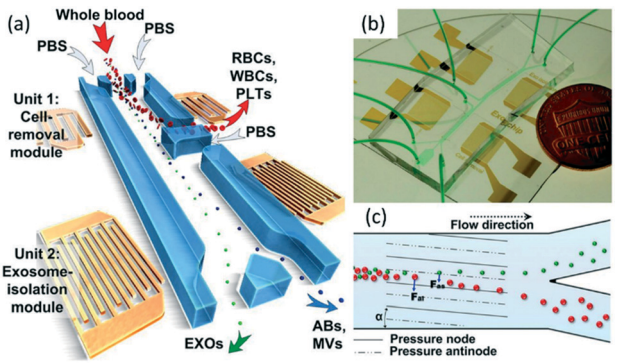

Fig. 8 Schematic illustration and mechanisms for isolating exosomes from blood using an acoustic microfluidic device.[163] (a) RBCs, WBCs, and PLTs are filtered by the cell-removal module, and then subgroups of EVs (ABs: apoptotic bodies; EXOs: exosomes; MVs: microvesicles) are separated. Reproduced from ref. 163. Copyright 2017, National Academy of Sciences, USA. (b) An optical image of the device. Two acoustic modules are integrated on a single chip. Reproduced from ref. 163. Copyright 2017, National Academy of Sciences, USA. (c) Size-based separation due to the lateral deflection induced by an acoustic field. The periodic distribution of pressure nodes and antinodes produces an acoustic radiation force to push larger particles toward node planes. Reproduced from ref. 163. Copyright 2017, National Academy of Sciences, USA.

Table 1 Summary of microfluidic techniques for focusing sub-micrometer particles

Classification	Method	Criteria	Sample	Size (μm)	Throughput	Merits	Demerits
Inertial focusing[50,54–56]	Inertial fluid	Size	PS particles, *E. coli*, *S. typhimurium* and *K. pneumoniae*	0.50 to 0.92	30 to 500 μL min^{-1}	High throughput	Low resolution
Viscoelastic microfluidics[65,68,69,71–73]	Viscoelastic fluid	Viscoelasticity and size	PS particles, *E. coli*, λ-DNA and T4-DNA, exosomes, microvesicles	0.10 to ~1.0	0.27 nL to 25 μL min^{-1}	Easy to operate	Particle–particle interactions
DLD[74,75,77,80]	DLD pillars	Size and shape	PS particles, DNA, *E. coli*, *S. epidermidis*, *K. pneumoniae* *P. aeruginosa*, exosomes	0.02 to 1.50	0.10 nL to 0.05 μL min^{-1}	High resolution and shape-dependent	Complex fabrication and anisotropic permeability
Hydrophoresis[124]	Anisotropic obstacles	Size	PS particles and DNA	0.52 to 1.10	0.01 μL min^{-1}	Easy control	Low throughput and clogging
DEP[26,87–89,91]	Non-uniform electric field	Polarizability and size	Silica, PS and WO_3 particles, *E. coli*, PSI crystals, λ-DNA	0.08 to 0.90	0.022 to 25 μL min^{-1}	High resolution and real-time control	Complicated preparation process and risk for sample damage
Acoustophoresis[97,108,63]	Acoustic field	Compressibility, acoustic properties, density and size	PS particles, exosomes, *E. coli*, chylomicrons, and lipoproteins	0.11 to 0.87	0.20 to 4.0 μL min^{-1}	Versatile and non-contact	Attenuation of acoustic waves
Thermophoresis[118]	Non-isothermal field	Size	PS particles	0.10 to 1.0	24 μL min^{-1} (10 mm s^{-1})	Non-contact	Risk of changes in structures
Optical tweezers[128]	Optical field	Size	N.A.	0.10 to 0.20	0.24 nL min^{-1}	No need for sheath flow and simple fabrication	Low throughput
DEP + DLD[137,138]	Non-uniform electric field + DLD pillars	Polarizability and size	Extracellular vesicles, PS particles	0.05 to 0.50	0.30 nL min^{-1}	Tuneable critical diameter	Low throughput
Inertial + thermophoresis[140]	Inertial fluid + non-isothermal field	Size	Fluorescent particles	0.50 to 1.0	N.A.	Non-contact	Low throughput

the ability of the acoustic focusing technique to integrate with the downstream separation components. We expect that this device can further advance exosome-related biomedical research with potential applications in health monitoring, disease diagnostics and therapeutics.

5.4 Design guidelines

The mechanisms underlying each technique are different, thus leading to the difficulties in the development of overall design guidelines for the focusing of sub-micrometer particles. Here, we summarize general design guidelines for each technique based on its operating principles.

In inertial microfluidics, required minimum channel length and flow rate should be designed to achieve effective focusing of particles to equilibrium positions in straight rectangular or continuously curving channels.[49] To avoid trade-off between these two parameters, using a channel with varying cross sections is a promising method.[55] For viscoelastic microfluidics, precise control of the rheological properties of the carrier solution is the key.[58] Critical diameter plays an essential role in a DLD device, so its design should focus on the physics between pillars. Moreover, the integration of DLD with external fields provides an alternative approach to promote focusing performance.[138] Appropriate anisotropic obstacles are used for hydrophoretic focusing, and the height of the obstacles need to be comparable to particle size.[125]

Non-uniform distributed electrical field is the key for DEP focusing, and careful design of electrode arrays within channels or insulating structures is necessary.[172] A general approach for effective focusing of small-sized particles by acoustophoresis is to use high-frequency acoustic radiation. Also, the layout of piezoelectric films needs to be considered. Particle focusing using thermophoresis is at a nascent stage, and several factors, such as temperature gradient, flow rate and channel geometry can affect thermophoretic focusing. The mechanism of focusing sub-micrometer particles using optical force is identical to optical tweezers.[128,173] Please refer to comprehensive and in-depth studies on inertial microfluidics,[49,55,56,174] viscoelastic microfluidics,[58,175,176] DLD,[76,138,177] hydrophoresis,[124,125] DEP,[172,178] acoustophoresis,[107,141,179] thermophoresis[118,180] and optical focusing[128,173] to obtain detailed design guidelines.

6. Conclusion

Due to the significance of sub-micrometer particles (*e.g.*, microvesicles, protein aggregates and *E. coli*) in various fields such as biology, biomedicine, chemistry and environment, the focusing of sub-micrometer particles, a prerequisite step for downstream detection, separation and manipulation, draws great interest in microfluidic devices. With improvements in theoretical fundamentals and fabrication technology, the focusing resolution has advanced from micrometer to sub-micrometer and even to nanometer scale. It also allows the integration of particle focusing techniques to lab-on-a-chip systems for wider applications.

In this work, eight main microfluidic techniques, either passive or active, for focusing sub-micrometer particles have been discussed along with hybrid methods. Their characteristics are summarized and compared in Table 1. The selection of the optimum approach usually depends on the needs of applications. Each microfluidic technique has its merits and demerits, for example, inertial microfluidics can achieve high throughput but it is limited by low focusing resolution. Further, hybrid microfluidics integrates the strength of each approach, making it attractive for particle focusing. Although great advances in sub-micrometer particle focusing have been achieved in microfluidic devices recently, it calls for further optimization of these techniques to improve focusing resolution, simplify sample preparation, reduce the risk of sample damage, enhance throughput, *etc.* for practical applications. We expect that better performance of sub-micrometer particle focusing in terms of accuracy, throughput and reproducibility can be achieved with future advances in microfluidic techniques.

Conflicts of interest

There are no conflicts to declare.

Acknowledgements

This work is supported by Amada Foundation and NSG Foundation of Japan and MQ-NAIST Cotutelle Program. We also acknowledge the support of JSPS Core-to-Core program and Macquarie University New Staff Grant.

References

1 J. Shi, S. Yazdi, S. C. S. Lin, X. Ding, I. K. Chiang, K. Sharp and T. J. Huang, *Lab Chip*, 2011, **11**, 2319–2324.
2 X. Xuan, J. Zhu and C. Church, *Microfluid. Nanofluid.*, 2010, **9**, 1–16.
3 N. Nitta, T. Sugimura, A. Isozaki, H. Mikami, K. Hiraki, S. Sakuma, T. Iino, F. Arai, T. Endo, Y. Fujiwaki, H. Fukuzawa, M. Hase, T. Hayakawa, K. Hiramatsu, Y. Hoshino, M. Inaba, T. Ito, H. Karakawa, Y. Kasai, K. Koizumi, S. Lee, C. Lei, M. Li, T. Maeno, S. Matsusaka, D. Murakami, A. Nakagawa, Y. Oguchi, M. Oikawa, T. Ota, K. Shiba, H. Shintaku, Y. Shirasaki, K. Suga, Y. Suzuki, N. Suzuki, Y. Tanaka, H. Tezuka, C. Toyokawa, Y. Yalikun, M. Yamada, M. Yamagishi, T. Yamano, A. Yasumoto, Y. Yatomi, M. Yazawa, D. Di Carlo, Y. Hosokawa, S. Uemura, Y. Ozeki and K. Goda, *Cell*, 2018, **175**, 266–276.e13.
4 C. Lei, H. Kobayashi, Y. Wu, M. Li, A. Isozaki, A. Yasumoto, H. Mikami, T. Ito, N. Nitta, T. Sugimura, M. Yamada, Y. Yatomi, D. Di Carlo, Y. Ozeki and K. Goda, *Nat. Protoc.*, 2018, **13**, 1603–1631.
5 K. Goda, A. Ayazi, D. R. Gossett, J. Sadasivam, C. K. Lonappan, E. Sollier, A. M. Fard, S. C. Hur, J. Adam, C. Murray, C. Wang, N. Brackbill, D. Di Carlo and B. Jalali, *Proc. Natl. Acad. Sci. U. S. A.*, 2012, **109**, 11630–11635.
6 D. R. Gossett, H. T. K. Tse, S. A. Lee, Y. Ying, A. G. Lindgren, O. O. Yang, J. Rao, A. T. Clark and D. Di Carlo, *Proc. Natl. Acad. Sci. U. S. A.*, 2012, **109**, 7630–7635.
7 H. T. K. Tse, D. R. Gossett, Y. S. Moon, M. Masaeli, M. Sohsman, Y. Ying, K. Mislick, R. P. Adams, J. Rao and D. Di Carlo, *Sci. Transl. Med.*, 2013, **5**, 212ra163.
8 S. H. Yang, D. J. Lee, J. R. Youn and Y. S. Song, *Anal. Chem.*, 2017, **89**, 3639–3647.
9 E. K. Sackmann, A. L. Fulton and D. J. Beebe, *Nature*, 2014, **507**, 181–189.
10 D. Mark, S. Haeberle, G. Roth, F. Von Stetten and R. Zengerle, *Chem. Soc. Rev.*, 2010, **39**, 1153–1182.
11 N. Ota, Y. Owa, T. Kawai and Y. Tanaka, *J. Chromatogr. A*, 2016, **1455**, 172–177.
12 A. M. Gañán-Calvo, J. M. Montanero, L. Martín-Banderas and M. Flores-Mosquera, *Adv. Drug Delivery Rev.*, 2013, **65**, 1447–1469.
13 K. S. Elvira, X. C. I. Solvas, R. C. R. Wootton and A. J. deMello, *Nat. Chem.*, 2013, **5**, 905–915.
14 W. Jung, J. Han, J. W. Choi and C. H. Ahn, *Microelectron. Eng.*, 2015, **132**, 46–57.
15 Y. Shen, Y. Yalikun and Y. Tanaka, *Sens. Actuators, B*, 2019, **282**, 268–281.
16 T. A. Brown, R. D. Fetter, A. N. Tkachuk and D. A. Clayton, *Methods*, 2010, **51**, 458–463.
17 M. Navratil, A. Terman and E. A. Arriaga, *Exp. Cell Res.*, 2008, **314**, 164–172.
18 H. S. Horowitz, S. J. Mclain, A. W. Sleight, J. D. Druliner, P. L. Gai, M. J. Vankavelaar, J. L. Wagner, B. D. Biggs and S. J. Poon, *Science*, 1989, **243**, 66–69.
19 S. Hong, J. Bhardwaj, C. H. Han and J. Jang, *Environ. Sci. Technol.*, 2016, **50**, 12365–12372.
20 C. J. Tan and Y. W. Tong, *Anal. Chem.*, 2007, **79**, 299–306.
21 T. Bollhorst, T. Grieb, A. Rosenauer, G. Fuller, M. Maas and K. Rezwan, *Chem. Mater.*, 2013, **25**, 3464–3471.
22 N. Lewinski, V. Colvin and R. Drezek, *Small*, 2008, **4**, 26–49.
23 S. Foss Hansen, B. H. Larsen, S. I. Olsen and A. Baun, *Nanotoxicology*, 2007, **1**, 243–250.
24 M. Auffan, J. Rose, J. Y. Bottero, G. V. Lowry, J. P. Jolivet and M. R. Wiesner, *Nat. Nanotechnol.*, 2009, **4**, 634–641.
25 R. Vasudev, S. Mathew and N. Afonina, *J. Pharm. Sci.*, 2015, **104**, 1622–1631.
26 B. G. Abdallah, T. C. Chao, C. Kupitz, P. Fromme and A. Ros, *ACS Nano*, 2013, **7**, 9129–9137.

27 M. Antfolk, P. B. Muller, P. Augustsson, H. Bruus and T. Laurell, *Lab Chip*, 2014, **14**, 2791–2799.
28 K. Lee, H. Shao, R. Weissleder and H. Lee, *ACS Nano*, 2015, **9**, 2321–2327.
29 S. EL Andaloussi, I. Mäger, X. O. Breakefield and M. J. A. Wood, *Nat. Rev. Drug Discovery*, 2013, **12**, 347–357.
30 B. György, T. G. Szabó, M. Pásztói, Z. Pál, P. Misják, B. Aradi, V. László, É. Pállinger, E. Pap, Á. Kittel, G. Nagy, A. Falus and E. I. Buzás, *Cell. Mol. Life Sci.*, 2011, **68**, 2667–2688.
31 M. A. Antonyak, B. Li, L. K. Boroughs, J. L. Johnson, J. E. Druso, K. L. Bryant, D. A. Holowka and R. A. Cerione, *Proc. Natl. Acad. Sci. U. S. A.*, 2011, **108**, 4852–4857.
32 E. Boilard, P. A. Nigrovic, K. Larabee, G. F. M. Watts, J. S. Coblyn, M. E. Weinblatt, E. M. Massarotti, E. Remold-O'Donnell, R. W. Farndale, J. Ware and D. M. Lee, *Science*, 2010, **327**, 580–583.
33 B. György, K. Módos, E. Pállinger, K. Pálóczi, M. Pásztói, P. Misják, M. A. Deli, A. Sipos, A. Szalai, I. Voszka, A. Polgár, K. Tóth, M. Csete, G. Nagy, S. Gay, A. Falus, A. Kittel and E. I. Buzás, *Blood*, 2011, **117**, e39–48.
34 C. Soto, L. Estrada and J. Castilla, *Trends Biochem. Sci.*, 2006, **31**, 150–155.
35 M. Jucker and L. C. Walker, *Nature*, 2013, **501**, 45–51.
36 C. Lin, R. Jungmann, A. M. Leifer, C. Li, D. Levner, G. M. Church, W. M. Shih and P. Yin, *Nat. Chem.*, 2012, **4**, 832–839.
37 M. Otto, *Nat. Rev. Microbiol.*, 2009, **7**, 555–567.
38 F. D. Lowy, *N. Engl. J. Med.*, 1998, **339**, 520–532.
39 A. Morel, Y. H. Ahn, F. Partensky, D. Vaulot and H. Claustre, *J. Mar. Res.*, 1993, **51**, 617–649.
40 F. Partensky, W. R. Hess and D. Vaulot, *Microbiol. Mol. Biol. Rev.*, 1999, **63**, 106–127.
41 E. T. Buitenhuis, W. K. W. Li, D. Vaulot, M. W. Lomas, M. R. Landry, F. Partensky, D. M. Karl, O. Ulloa, L. Campbell, S. Jacquet, F. Lantoine, F. Chavez, D. Macias, M. Gosselin and G. B. McManus, *Earth Syst. Sci. Data*, 2012, **4**, 37–46.
42 S. J. Biller, P. M. Berube, D. Lindell and S. W. Chisholm, *Nat. Rev. Microbiol.*, 2015, **13**, 13–27.
43 S. W. Chisholm, *Curr. Biol.*, 2017, **27**, R447–R448.
44 G. M. Hennon, J. J. Morris, S. T. Haley, E. R. Zinser, A. R. Durrant, E. Entwistle, T. Dokland and S. T. Dyhrman, *ISME J.*, 2018, **12**, 520–531.
45 N. Joumaa, M. Lansalot, A. Théretz, A. Elaissari, A. Sukhanova, M. Artemyev, I. Nabiev and J. H. M. Cohen, *Langmuir*, 2006, **22**, 1810–1816.
46 C. Loos, T. Syrovets, A. Musyanovych, V. Mailänder, K. Landfester, G. U. Nienhaus and T. Simmet, *Beilstein J. Nanotechnol.*, 2014, **5**, 2403–2412.
47 A. Rogach, A. Susha, F. Caruso, G. Sukhorukov, A. Kornowski, S. Kershaw, H. Möhwald, A. Eychmüller and H. Weller, *Adv. Mater.*, 2000, **12**, 333–337.
48 S. W. Ahn, S. S. Lee, S. J. Lee and J. M. Kim, *Chem. Eng. Sci.*, 2015, **126**, 237–243.
49 D. Di Carlo, *Lab Chip*, 2009, **9**, 3038–3046.
50 L. Wang and D. S. Dandy, *Adv. Sci.*, 2017, **4**, 1700153.
51 M. Li, M. van Zee, K. Goda and D. Di Carlo, *Lab Chip*, 2018, **18**, 2575–2582.
52 M. Li, H. E. Muñoz, A. Schmidt, B. Guo, C. Lei, K. Goda and D. Di Carlo, *Lab Chip*, 2016, **16**, 4458–4465.
53 J. M. Martel and M. Toner, *Annu. Rev. Biomed. Eng.*, 2014, **16**, 371–396.
54 J. Cruz, S. Hooshmand Zadeh, T. Graells, M. Andersson, J. Malmström, Z. G. Wu and K. Hjort, *J. Micromech. Microeng.*, 2017, **27**, 084001.
55 B. R. Mutlu, J. F. Edd and M. Toner, *Proc. Natl. Acad. Sci. U. S. A.*, 2018, **115**, 7682–7687.
56 J. Cruz, T. Graells, M. Walldén and K. Hjort, *Lab Chip*, 2019, **19**, 1257–1266.
57 Y. Gou, Y. Jia, P. Wang and C. Sun, *Sensors*, 2018, **18**, 1762.
58 A. M. Leshansky, A. Bransky, N. Korin and U. Dinnar, *Phys. Rev. Lett.*, 2007, **98**, 234501.
59 E. S. Asmolov, *J. Fluid Mech.*, 1999, **381**, 63–87.
60 S. Yang, J. Y. Kim, S. J. Lee, S. S. Lee and J. M. Kim, *Lab Chip*, 2011, **11**, 266–273.
61 R. J. Poole, *The Deborah and Weissenberg numbers*, 2012, vol. 53.
62 D. Yuan, Q. Zhao, S. Yan, S. Y. Tang, G. Alici, J. Zhang and W. Li, *Lab Chip*, 2018, **18**, 551–567.
63 J. Zhang, S. Yan, D. Yuan, G. Alici, N. T. Nguyen, M. Ebrahimi Warkiani and W. Li, *Lab Chip*, 2016, **16**, 10–34.
64 T. M. Squires and S. R. Quake, *Rev. Mod. Phys.*, 2005, **77**, 977–1026.
65 J. Y. Kim, S. W. Ahn, S. S. Lee and J. M. Kim, *Lab Chip*, 2012, **12**, 2807–2814.
66 K. Sozański, A. Wiśniewska, T. Kalwarczyk and R. Hołyst, *Phys. Rev. Lett.*, 2013, **111**, 228301.
67 A. Nikoubashman, N. A. Mahynski, A. H. Pirayandeh and A. Z. Panagiotopoulos, *J. Chem. Phys.*, 2014, **140**, 094903.
68 I. De Santo, G. D'Avino, G. Romeo, F. Greco, P. A. Netti and P. L. Maffettone, *Phys. Rev. Appl.*, 2014, **2**, 064001.
69 C. Liu, C. Xue, X. Chen, L. Shan, Y. Tian and G. Hu, *Anal. Chem.*, 2015, **87**, 6041–6048.
70 C. Liu, B. Ding, C. Xue, Y. Tian, G. Hu and J. Sun, *Anal. Chem.*, 2016, **88**, 12547–12553.
71 C. Liu, J. Guo, F. Tian, N. Yang, F. Yan, Y. Ding, J. Wei, G. Hu, G. Nie and J. Sun, *ACS Nano*, 2017, **11**, 6968–6976.
72 C. Liu, J. Zhao, F. Tian, J. Chang, W. Zhang and J. Sun, *J. Am. Chem. Soc.*, 2019, **141**, 3817–3821.
73 Y. Zhou, Z. Ma, M. Tayebi and Y. Ai, *Anal. Chem.*, 2019, **91**, 4577–4584.
74 K. K. Zeming, N. V. Thakor, Y. Zhang and C. H. Chen, *Lab Chip*, 2016, **16**, 75–85.
75 L. R. Huang, E. C. Cox, R. H. Austin and J. C. Sturm, *Science*, 2004, **304**, 987–990.
76 J. McGrath, M. Jimenez and H. Bridle, *Lab Chip*, 2014, **14**, 4139–4158.
77 S. Ranjan, K. K. Zeming, R. Jureen, D. Fisher and Y. Zhang, *Lab Chip*, 2014, **14**, 4250–4262.
78 S. M. Santana, M. A. Antonyak, R. A. Cerione and B. J. Kirby, *Biomed. Microdevices*, 2014, **16**, 869–877.

79 J. C. Sturm, E. C. Cox, B. Comella and R. H. Austin, *Interface Focus*, 2014, **4**, 20140054.
80 B. H. Wunsch, J. T. Smith, S. M. Gifford, C. Wang, M. Brink, R. L. Bruce, R. H. Austin, G. Stolovitzky and Y. Astier, *Nat. Nanotechnol.*, 2016, **11**, 936–940.
81 S. C. Kim, B. H. Wunsch, H. Hu, J. T. Smith, R. H. Austin and G. Stolovitzky, *Proc. Natl. Acad. Sci. U. S. A.*, 2017, **114**, E5034–E5041.
82 R. Vernekar, T. Krüger, K. Loutherback, K. Morton and D. W. Inglis, *Lab Chip*, 2017, **17**, 3318–3330.
83 S. Fiedler, S. G. Shirley, T. Schnelle and G. Fuhr, *Anal. Chem.*, 1998, **70**, 1909–1915.
84 P. R. C. Gascoyne and J. Vykoukal, *Electrophoresis*, 2002, **23**, 1973–1983.
85 R. Martinez-Duarte, *Electrophoresis*, 2012, **33**, 3110–3132.
86 S. Ozuna-Chacón, B. H. Lapizco-Encinas, M. Rito-Palomares, S. O. Martínez-Chapa and C. Reyes-Betanzo, *Electrophoresis*, 2008, **29**, 3115–3122.
87 A. A. Kayani, C. Zhang, K. Khoshmanesh, J. L. Campbell, A. Mitchell and K. Kalantar-zadeh, *Electrophoresis*, 2010, **31**, 1071–1079.
88 A. F. Chrimes, A. A. Kayani, K. Khoshmanesh, P. R. Stoddart, P. Mulvaney, A. Mitchell and K. Kalantar-zadeh, *Lab Chip*, 2011, **11**, 921–928.
89 S. Park, Y. Zhang, T. H. Wang and S. Yang, *Lab Chip*, 2011, **11**, 2893–2900.
90 M. Kim, T. Jung, Y. Kim, C. Lee, K. Woo, J. H. Seol and S. Yang, *Biosens. Bioelectron.*, 2015, **74**, 1011–1015.
91 P. V. Jones, G. L. Salmon and A. Ros, *Anal. Chem.*, 2017, **89**, 1531–1539.
92 Z. Rozynek, M. Han, F. Dutka, P. Garstecki, A. Józefczak and E. Luijten, *Nat. Commun.*, 2017, **8**, 15255.
93 B. H. Lapizco-Encinas, B. A. Simmons, E. B. Cummings and Y. Fintschenko, *Anal. Chem.*, 2004, **76**, 1571–1579.
94 L. Wu, L. Y. Lanry Yung and K. M. Lim, *Biomicrofluidics*, 2012, **6**, 14113.
95 M. Koklu, S. Park, S. D. Pillai and A. Beskok, *Biomicrofluidics*, 2010, **4**, 034107.
96 S. H. Liao, C. Y. Chang and H. C. Chang, *Biomicrofluidics*, 2013, **7**, 24110.
97 L. Liu, K. Chen, N. Xiang and Z. Ni, *Electrophoresis*, 2019, **40**, 873–889.
98 Q. Chen and Y. J. Yuan, *RSC Adv.*, 2019, **9**, 4963–4981.
99 R. Pethig, *J. Electrochem. Soc.*, 2017, **164**, B3049–B3055.
100 B. H. Lapizco-Encinas, *Electrophoresis*, 2017, **38**, 1405–1406.
101 V. Yantchev, J. Enlund, I. Katardjiev and L. Johansson, *J. Micromech. Microeng.*, 2010, **20**, 035031.
102 G. Destgeer, B. H. Ha, J. H. Jung and H. J. Sung, *Lab Chip*, 2014, **14**, 4665–4672.
103 D. J. Collins, Z. Ma and Y. Ai, *Anal. Chem.*, 2016, **88**, 5513–5522.
104 S. M. Woodside, B. D. Bowen and J. M. Piret, *AIChE J.*, 1997, **43**, 1727–1736.
105 H. Bruus, *Lab Chip*, 2012, **12**, 1014–1021.
106 X. Ding, S. C. S. Lin, B. Kiraly, H. Yue, S. Li, I. K. Chiang, J. Shi, S. J. Benkovic and T. J. Huang, *Proc. Natl. Acad. Sci. U. S. A.*, 2012, **109**, 11105–11109.
107 L. Y. Yeo and J. R. Friend, *Annu. Rev. Fluid Mech.*, 2014, **46**, 379–406.
108 J. Shi, H. Huang, Z. Stratton, Y. Huang and T. J. Huang, *Lab Chip*, 2009, **9**, 3354–3359.
109 J. Shi, X. Mao, D. Ahmed, A. Colletti and T. J. Huang, *Lab Chip*, 2008, **8**, 221–223.
110 D. J. Collins, T. Alan and A. Neild, *Lab Chip*, 2014, **14**, 1595–1603.
111 G. P. Gautam, R. Gurung, F. A. Fencl and M. E. Piyasena, *Anal. Bioanal. Chem.*, 2018, **410**, 6561–6571.
112 S. Li, F. Ma, H. Bachman, C. E. Cameron, X. Zeng and T. J. Huang, *J. Micromech. Microeng.*, 2017, **27**, 015031.
113 M. Wu, C. Chen, Z. Wang, H. Bachman, Y. Ouyang, P. H. Huang, Y. Sadovsky and T. J. Huang, *Lab Chip*, 2019, **19**, 1174–1182.
114 W. Connacher, N. Zhang, A. Huang, J. Mei, S. Zhang, T. Gopesh and J. Friend, *Lab Chip*, 2018, **18**, 1952–1996.
115 P. S. Epstein, *Z. Phys.*, 1929, **54**, 537–563.
116 J. R. Brock, *J. Colloid Sci.*, 1962, **17**, 768–780.
117 L. Talbot, R. K. Cheng, R. W. Schefer and D. R. Willis, *J. Fluid Mech.*, 1980, **101**, 737–758.
118 R. Wang, J. Du, W. Guo and Z. Zhu, *Nanoscale Microscale Thermophys. Eng.*, 2016, **20**, 51–65.
119 G. S. McNab and A. Meisen, *J. Colloid Interface Sci.*, 1973, **44**, 339–346.
120 M. Eslamian, *Front. Heat Mass Transfer*, 2011, **2**, 1–20.
121 M. Eslamian and M. Z. Saghir, *Appl. Therm. Eng.*, 2013, **59**, 527–534.
122 Y. Zhou, C. Yang, Y. C. Lam and X. Huang, *Int. J. Heat Mass Transfer*, 2016, **101**, 1283–1291.
123 E. H. Hill, J. Li, L. Lin, Y. Liu and Y. Zheng, *Langmuir*, 2018, **34**, 13252–13262.
124 S. Choi, S. Song, C. Choi and J. K. Park, *Anal. Chem.*, 2009, **81**, 50–55.
125 S. Song and S. Choi, *J. Chromatogr. A*, 2013, **1302**, 191–196.
126 D. G. Grier, *Nature*, 2003, **424**, 810–816.
127 K. Dholakia and T. Čižmár, *Nat. Photonics*, 2011, **5**, 335–342.
128 Y. Zhao, B. S. Fujimoto, G. D. Jeffries, P. G. Schiro and D. T. Chiu, *Opt. Express*, 2007, **15**, 6167–6176.
129 T. Zhu, R. Cheng and L. Mao, *Microfluid. Nanofluid.*, 2011, **11**, 695–701.
130 R. Afshar, Y. Moser, T. Lehnert and M. A. M. Gijs, *Anal. Chem.*, 2011, **83**, 1022–1029.
131 J. Zeng, C. Chen, P. Vedantam, V. Brown, T. R. J. Tzeng and X. Xuan, *J. Micromech. Microeng.*, 2012, **22**, 105018.
132 R. Zhou and C. Wang, *Biomicrofluidics*, 2016, **10**, 034101.
133 S. M. Kenyon, M. M. Meighan and M. A. Hayes, *Electrophoresis*, 2011, **32**, 482–493.
134 T. Kawamata, M. Yamada, M. Yasuda and M. Seki, *Electrophoresis*, 2008, **29**, 1423–1430.
135 S. Yan, J. Zhang, Y. Yuan, G. Lovrecz, G. Alici, H. Du, Y. Zhu and W. Li, *Electrophoresis*, 2015, **36**, 284–291.

136 S. Yan, J. Zhang, D. Yuan and W. Li, *Electrophoresis*, 2017, **38**, 238–249.
137 Y. Hattori, T. Shimada, T. Yasui, N. Kaji and Y. Baba, *Anal. Chem.*, 2019, **91**, 6514–6521.
138 V. Calero, P. Garcia-Sanchez, C. Honrado, A. Ramos and H. Morgan, *Lab Chip*, 2019, **19**, 1386–1396.
139 J. P. Beech, P. Jönsson and J. O. Tegenfeldt, *Lab Chip*, 2009, **9**, 2698–2706.
140 R. Wang, S. Sun, W. Wang and Z. Zhu, *Int. J. Heat Mass Transfer*, 2019, **133**, 912–919.
141 Y. Q. Fu, J. K. Luo, N. T. Nguyen, A. J. Walton, A. J. Flewitt, X. Zu, Y. Li, G. McHale, A. Matthews, E. Iborra, H. Du and W. I. Milne, *Prog. Mater. Sci.*, 2017, **89**, 31–91.
142 M. A. Croxen, R. J. Law, R. Scholz, K. M. Keeney, M. Wlodarska and B. B. Finlay, *Clin. Microbiol. Rev.*, 2013, **26**, 822–880.
143 N. Ota, Y. Yalikun, T. Suzuki, S. W. Lee, Y. Hosokawa, K. Goda and Y. Tanaka, *R. Soc. Open Sci.*, 2019, **6**, 181776.
144 M. Li, H. E. Muñoz, K. Goda and D. Di Carlo, *Sci. Rep.*, 2017, **7**, 10802.
145 M. Masaeli, E. Sollier, H. Amini, W. Mao, K. Camacho, N. Doshi, S. Mitragotri, A. Alexeev and D. Di Carlo, *Phys. Rev. X*, 2012, **2**, 031017.
146 J. J. Lee, K. J. Jeong, M. Hashimoto, A. H. Kwon, A. Rwei, S. A. Shankarappa, J. H. Tsui and D. S. Kohane, *Nano Lett.*, 2014, **14**, 1–5.
147 Ö. Baltekin, A. Boucharin, E. Tano, D. I. Andersson and J. Elf, *Proc. Natl. Acad. Sci. U. S. A.*, 2017, **114**, 9170–9175.
148 J. Skog, T. Würdinger, S. van Rijn, D. H. Meijer, L. Gainche, M. Sena-Esteves, W. T. Curry, B. S. Carter, A. M. Krichevsky and X. O. Breakefield, *Nat. Cell Biol.*, 2008, **10**, 1470–1476.
149 P. D. Robbins and A. E. Morelli, *Nat. Rev. Immunol.*, 2014, **14**, 195–208.
150 B. T. Pan, K. Teng, C. Wu, M. Adam and R. M. Johnstone, *J. Cell Biol.*, 1985, **101**, 942–948.
151 L. Barile and G. Vassalli, *Pharmacol. Ther.*, 2017, **174**, 63–78.
152 M. Tkach and C. Théry, *Cell*, 2016, **164**, 1226–1232.
153 K. W. Witwer, E. I. Buzás, L. T. Bemis, A. Bora, C. Lässer, J. Lötvall, E. N. Nolte-'t Hoen, M. G. Piper, S. Sivaraman, J. Skog, C. Théry, M. H. Wauben and F. Hochberg, *J. Extracell. Vesicles*, 2013, **2**, 20360.
154 K. K. Jella, T. H. Nasti, Z. Li, S. R. Malla, Z. S. Buchwald and M. K. Khan, *Vaccines*, 2018, **6**, 69.
155 R. C. Lai, R. W. Y. Yeo, K. H. Tan and S. K. Lim, *Biotechnol. Adv.*, 2013, **31**, 543–551.
156 J. C. Contreras-Naranjo, H. J. Wu and V. M. Ugaz, *Lab Chip*, 2017, **17**, 3558–3577.
157 P. Li, M. Kaslan, S. H. Lee, J. Yao and Z. Gao, *Theranostics*, 2017, **7**, 789–804.
158 T. Salafi, K. K. Zeming and Y. Zhang, *Lab Chip*, 2017, **17**, 11–33.
159 L. Rems, D. Kawale, L. J. Lee and P. E. Boukany, *Biomicrofluidics*, 2016, **10**, 043403.
160 J. L. Viovy, *Rev. Mod. Phys.*, 2000, **72**, 813–872.
161 M. Viefhues, J. Regtmeier and D. Anselmetti, *Analyst*, 2013, **138**, 186–196.
162 D. J. Beebe, G. A. Mensing and G. M. Walker, *Annu. Rev. Biomed. Eng.*, 2002, **4**, 261–286.
163 M. Wu, Y. Ouyang, Z. Wang, R. Zhang, P. H. Huang, C. Chen, H. Li, P. Li, D. Quinn, M. Dao, S. Suresh, Y. Sadovsky and T. J. Huang, *Proc. Natl. Acad. Sci. U. S. A.*, 2017, **114**, 10584–10589.
164 Y. Chen, A. J. Chung, T. H. Wu, M. A. Teitell, D. Di Carlo and P. Y. Chiou, *Small*, 2014, **10**, 1746–1751.
165 E. Ozkumur, A. M. Shah, J. C. Ciciliano, B. L. Emmink, D. T. Miyamoto, E. Brachtel, M. Yu, P. Chen, B. Morgan, J. Trautwein, A. Kimura, S. Sengupta, S. L. Stott, N. M. Karabacak, T. A. Barber, J. R. Walsh, K. Smith, P. S. Spuhler, J. P. Sullivan, R. J. Lee, D. T. Ting, X. Luo, A. T. Shaw, A. Bardia, L. V. Sequist, D. N. Louis, S. Maheswaran, R. Kapur, D. A. Haber and M. Toner, *Sci. Transl. Med.*, 2013, **5**, 179ra47.
166 T. H. Wu, Y. Chen, S. Y. Park, J. Hong, T. Teslaa, J. F. Zhong, D. Di Carlo, M. A. Teitell and P. Y. Chiou, *Lab Chip*, 2012, **12**, 1378.
167 S. Sakuma, Y. Kasai, T. Hayakawa and F. Arai, *Lab Chip*, 2017, **17**, 2760–2767.
168 X. Zhu, Y. C. Kung, T. H. Wu, M. A. Teitell and P. Y. E. Chiou, in *Optical Trapping and Optical Micromanipulation XIV*, ed. K. Dholakia and G. C. Spalding, SPIE, 2017, vol. 10347, p. 91.
169 L. Ren, S. Yang, P. Zhang, Z. Qu, Z. Mao, P. H. Huang, Y. Chen, M. Wu, L. Wang, P. Li and T. J. Huang, *Small*, 2018, **14**, 1801996.
170 O. Jakobsson, C. Grenvall, M. Nordin, M. Evander and T. Laurell, *Lab Chip*, 2014, **14**, 1943–1950.
171 K. S. Lee, M. Palatinszky, F. C. Pereira, J. Nguyen, V. I. Fernandez, A. J. Mueller, F. Menolascina, H. Daims, D. Berry, M. Wagner and R. Stocker, *Nat. Microbiol.*, 2019, **4**, 1035–1048.
172 B. Çetin and D. Li, *Electrophoresis*, 2011, **32**, 2410–2427.
173 J. R. Moffitt, Y. R. Chemla, S. B. Smith and C. Bustamante, *Annu. Rev. Biochem.*, 2008, **77**, 205–228.
174 H. Amini, W. Lee and D. Di Carlo, *Lab Chip*, 2014, **14**, 2739.
175 D. Stoecklein and D. Di Carlo, *Anal. Chem.*, 2019, **91**, 296–314.
176 G. D'Avino, F. Greco and P. L. Maffettone, *Annu. Rev. Fluid Mech.*, 2017, **49**, 341–360.
177 D. W. Inglis, J. A. Davis, R. H. Austin and J. C. Sturm, *Lab Chip*, 2006, **6**, 655–658.
178 S. Dash and S. Mohanty, *Electrophoresis*, 2014, **35**, 2656–2672.
179 J. Friend and L. Y. Yeo, *Rev. Mod. Phys.*, 2011, **83**, 647–704.
180 Z. Liu, Z. Chen and M. Shi, *Appl. Therm. Eng.*, 2009, **29**, 1020–1025.